Chapter 2

Phase Diagram Exhibiting a Smectic A – Smectic C – Smectic F Meeting Point

Phase diagram exhibiting a Sm A-Sm C-Sm F point

2.1 Introduction

Thermally excited fluctuations are expected to prevent 2D XY systems from exhibiting a phase transition above zero kelvin. However, Kosterlitz and Thouless' (KT) demonstrated that one can define a phase transition in terms of defects present in the system. Examples of systems thought to exhibit such KT transitions are certain planar magnets, films of liquid helium, thin superconducting films, gases adsorbed on crystal surfaces and certain liquid crystalline transitions. These transitions would be mediated by the unbinding of paired defects. Halperin and Nelson[2] and independently Young[3] recognised that in 2D crystals melting would occur in two stages. In the first step lattice dislocations (see figure 2.1a) would unbind leading to disruption of the positional order. But the long range coherence of the orientation of the local crystallographic axes still persists. The resulting order has been referred to as bond orientational order (BOO). The bond between the nearest neighbour is not a chemical bond but merely a geometric line. The second stage of melting is due to disclination - defect associated with the orientation of the lattice (see figure 2.1b). In the case of a two dimensional hexagonal lattice disclinations may be of either five fold or seven fold symmetry. In the bond orientational ordered phase, referred to as the hexatic phase, these two types of disclinations would exist as bound pairs. The unbinding of these disclinations would result in a two-dimensional fluid phase with continuous rotational and translational symmetry. The 2D hexatic phase has short ranged positional order but quasi long ranged six fold BOO.

These predictions prompted the search for the intermediate hexatic phase.

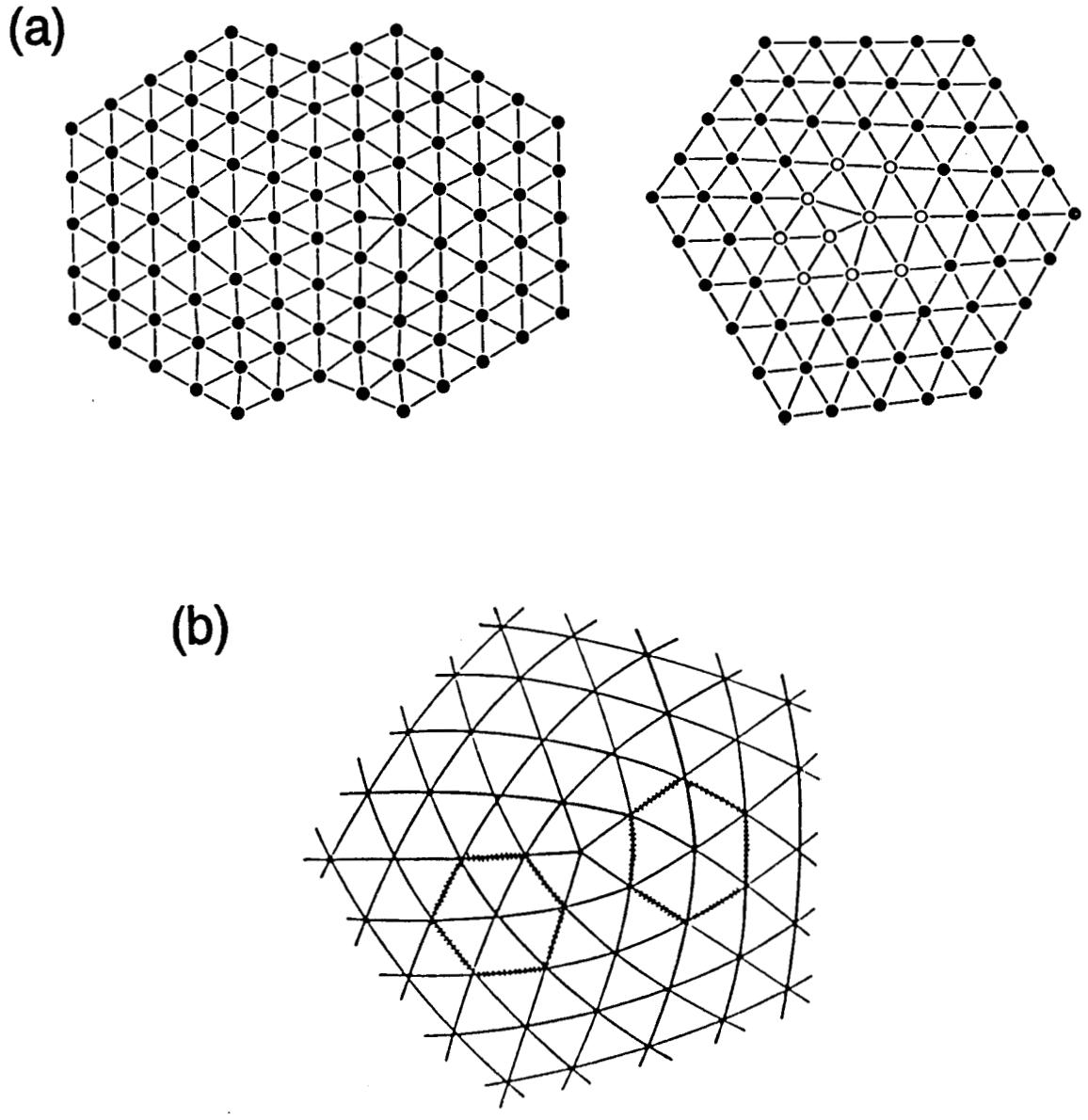

Figure 2.1: Lattice defects in a two-dimensional triangular lattice. (a) Left: An isolated dislocation. Picture to the right shows a bound pair of dislocations-two dislocations with opposite Burgers vector. (b) A disclination defect.

By considering the following arguments, Birgeneau and Litster[4] put forward a profound idea which led to the discovery of hexatic liquid crystals. The smectic phases are layered, and can be thought of as layers of two-dimensional phases stacked on one another. If the stacks are of two-dimensional solids then infinitesimal interactions would lead to a long-range positional order and a three dimensional crystal. If instead the stacks are two-dimensional liquids, the resulting phase would be a smectic **A** phase with a one-dimensional density modulation and an in-plane liquid-like order, as mentioned earlier. If the layers are **hexatic** the algebraically decaying correlation function in a 2-d hexatic *sheet* implies an infinite susceptibility to an external coupling. Such a coupling, even if infinitesimally small, would drive the algebraically decaying BOO to long range order. Such a phase would have a one-dimensional density modulation and a three-dimensional BOO. It was further suggested that the bulk smectic B phase may be understood as a three dimensional generalisation of the hexatic liquid crystal phase, consisting of two dimensional hexatic layers which interact to produce long range, three dimensional BOO, i.e., a stacked hexatic phase, with short range positional order of the molecules within the layers. If this analogy is correct, then the smcctic B-smectic **A** transition would be an example of the disclination unbinding transition. Experimental identification of the existence of such a phase requires sophisticated tools. Since X-ray diffraction studies have been responsible for its discovery we will mention here the X-ray signature of the hexatic phase. Figure 2.2 shows schematic diagram of the in-plane scattering from such a phase along with those for two-dimensional liquids (smectic A [Sm **A**]) and solids (crystal B [Cry B]). The scattering remains diffuse, just like

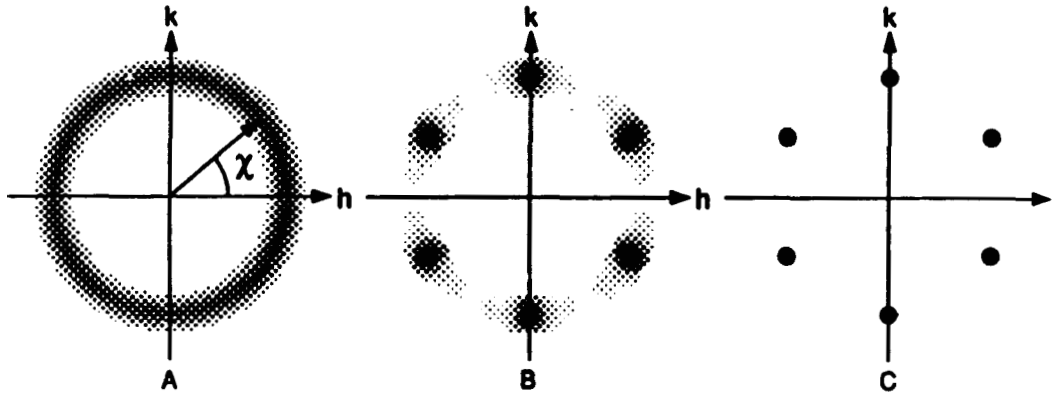

Figure 2.2: Schematic representation of tlie in-plane X-ray scatteririg profile expected for (A) two-dimensional liquid(Sm A), (B) hexatic B and (C) Crystal B phases.

in the Sm **A** phase, but develops 6-fold modulation in the angle χ. Moncton and Pindak's[5] first set of experiments showed that, contrary to the hypothesis of Birgeneau and Litster,[4] the smectic B phase found in the liquid crystal compound called 40.8 has three dimensional long-range positional order and is therefore a true crystalline phase (known as Crystal B or Cry B). Cry B phase has its constituent molecules arranged in hexagonally closely packed array within the layers, with the long axis of the molecules being perpendicular to the layer planes. Both BOO and positional orders are long range within the layers. The discovery of the liquid crystalline hexatic phase was reported first by Pindak, Moncton, Davey and Goodby.[6] Using free standing liquid crystal film techniques they showed that the material 65OBC possessed a three dimensionally stacked hexatic B (hex B) phase. The hex B phase has long range 6-fold BOO, short range in-plane positional correlations and no interlayer correlations. Just like in the Cry B phase the molecules are oriented along the layer normal direction. Apart from this orthogonal hexatic phase, tilted forms of hexatic phases viz., smectic I (Sm I) and smectic F (Sm F) have also been observed. Sm F and Sm I phases differ in the direction of tilt (see figure **2.3).** The projection of the director onto the smectic planes points towards a near-neighbour in the Sm I phase and between two near-neighbours in the Sm F phase. Crystalline versions of the Sm I and Sm F phases are called crystal J (Cry J) and crystal G (Cry G) phases respectively. At this point it should be noted that the coupling to the molecular tilt is expected'to induce long range hexatic order even in the smectic C phase.[7] Important insights regarding the structure of the tilted hexatic phase Sm I and the nature of the Sm C-Sm I transitions were obtained in a recent

Phase diagram exhibiting a Sm A-Sm C-Sm *F* point

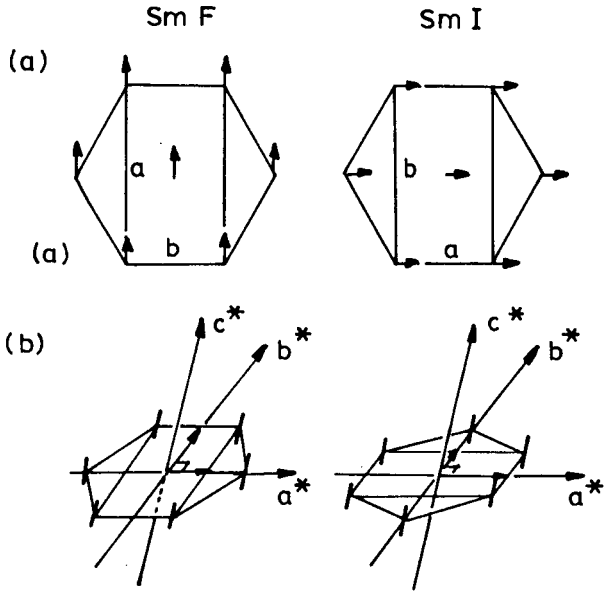

Figure **2.3:** (a) Molecular packing within the layer plane of Sm F and Sm I phases. The arrows represent the projection of the molecular tilt on to this plane. (b) Reciprocal lattice picture of the arrangement shown in (a).

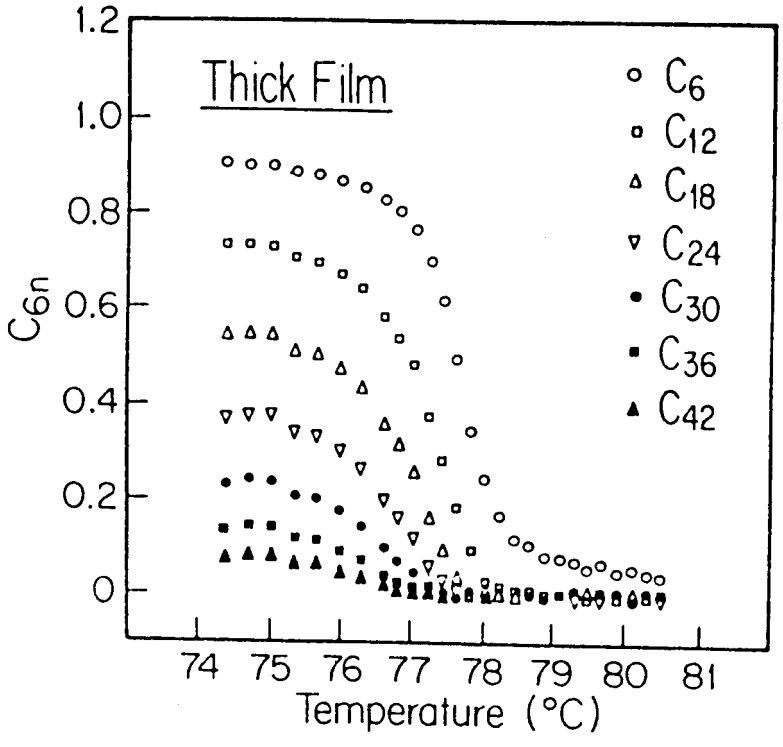

Figure 2.4: Temperature dependence of tho different Fourier coefficients describing the hexatic ordering in a thick film of 8OSI. (From Ref. 8.)

synchrotron X-ray experiment.[8] Quantitative information about the BO order was extracted by describing the X-ray structure using an expression

$$S(\chi) = I_o\left[1/2 + \sum_{n=1}^{\infty} C_{6n} \cos 6n(90^o - \chi)\right] - I_{BG} \qquad (2.1)$$

Here χ is the angle between the in-plane component of the scattering vector and an external reference axis. The coefficients C_{6n} measure the amount of 6n-fold ordering in the sample. Figure 2.4 shows the temperature dependence of the different Fourier coefficients C_{6n} in a sample of 8OSI. The absence of a sharp boundary between Sm C and Sm I phases is indicative of the continuous evolution nature of the transition. The first coefficient C_6 is the primary order parameter and each of the higher harmonics behaves like a secondary order parameter. Very interesting physics has emerged as each of these order parameters exhibit a different symmetry.

Theoretically,[7,9–10] a number of topologies for the phase diagram involving different hexatic phases have been worked out. A mean-field phase diagram proposed by Bruinsma and Nelson[7] is shown in figure 2.5. The phases involved, Sm A, smectic C (Sm C) and hex B are seen to be meeting at a point. In this model, all the three transitions are second order and are 3-d XY like (i.e., they belong to the same universality class as the superfluid-normal transition in He^4). The meeting point is a multicriticai point. Aharony et al.,[9] have discussed a phase diagram in the temperature-concentration plane (see figure 2.6) involving Sm A, hex B and Cry B phases. It is seen that the meeting point of these phases is a triple point due to the existence of a tricritical point on the Sm A-hex B boundary. (A triple point is the point at which three first order

Phase diagram exhibiting a Sm A-Sm C-Sm F point

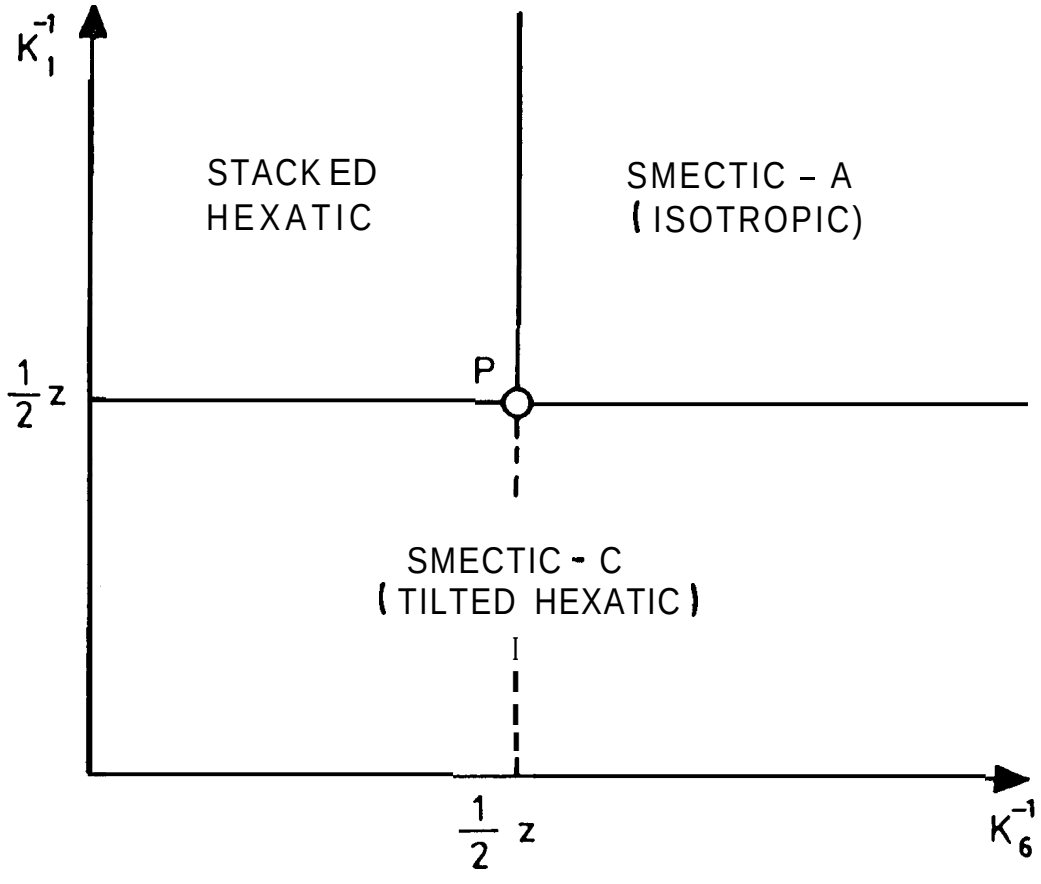

Figure 2.5: Phase diagram of a coupled system of bond- and tilt orientation angles in the mean-field approximation. Three XY-like lines of critical points separate different phases and meet at the multicritical point P. Here K_6 measures the coupling between neighbouring bond orientations, while K_1 characterizes the interaction between nearby tilt angles. (From Bruinsrna and Nelson of Ref. 7)

Phase diagram exhibiting a Sm *A-Sm C-Sm F* point

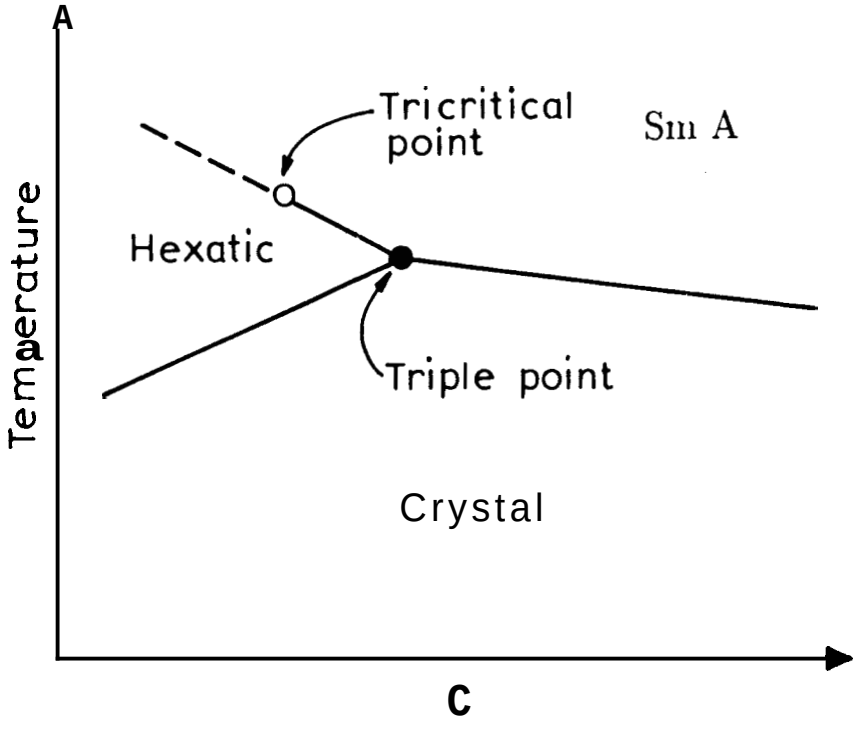

Figure 2.6: Generic temperature-concentration phase diagram near the Sm A-hex B-Cry B point. The broken(full) lines indicate second-(first-) order transitions. (From Ref. 9).

lines meet and all the three phases coexist. A tricritical point is one at which the order of transition changes over from first order to second order). More recently, Defontaines and Prost[11] have proposed a variety of scenarios involving Sm A, hex B, Sm C and Sm I phases.

On the experimental side, very few phase diagrams have been studied in detail. Heat capacity measurements by Pitchford et al.,[12] showed a meeting point of Sm A-hex B-Sm I phases in a binary system (see figure 2.7). Nounesis et al.,[13] observed a meeting point of Sm A, hex B and Cry E phases in a binary liquid crystalline system (see figure 2.8). The meeting point turned out to be a triple point with a tricritical point on the Sm A-hex B boundary. High pressure measurements[14] conducted very recently in our laboratory showed different types of meeting points viz., Sm A-Sm C-hex B, Sm A-Sm C-Cry B points (see Figures 2.9a & b). However, no theoretical or experimental phase diagrams with Sm A, Sm C and a tilted hexatic phase (Sm F or Sm I) have been reported. At this point it may be relevant to comment on certain factors regarding the nature of phase transition between these phases.

- The Sm A-Sm C phase transition is described by a two component complex order parameter[15] $\Theta = \theta\, e^{i\phi}$ where θ is the magnitude of tilt angle and ϕ, the azimuthal angle (see Figure 2.10). Since ϕ can be chosen arbitrarily, θ itself is taken as the order parameter in the free energy expansion for the Sm A-Sm C transition. From symmetry consideration Sm A-Sm C phase transition can be either first order or second order. Experimentally this transition is generally found to be second order. Based on heat capacity

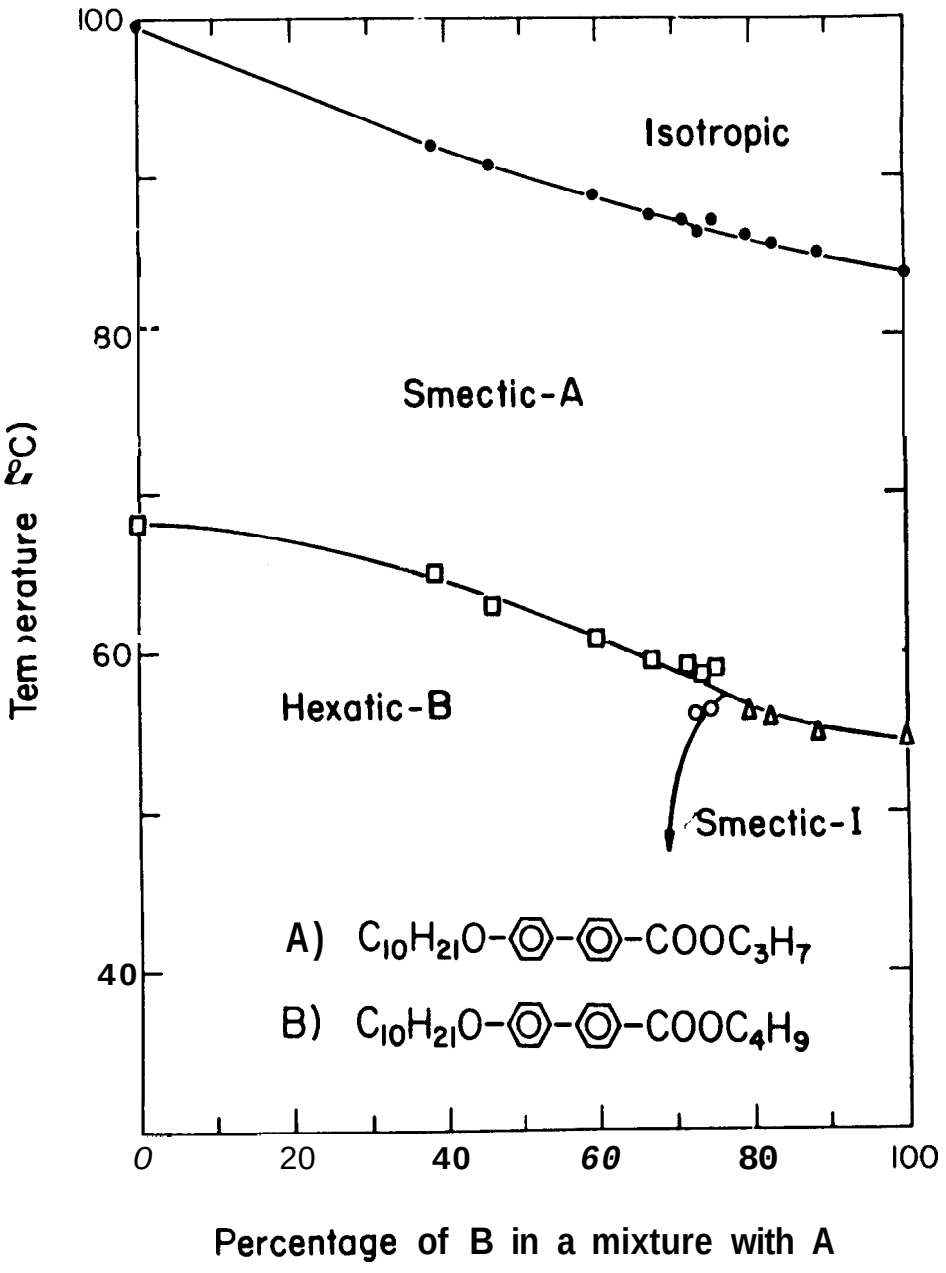

Figure 2.7: Temperature-concentration phase diagram of 3(10)OBC and 4(10)OBC mixtures showing a Sm A-hex B-Sm 1 meeting point.
(From Ref. 12).

Phase *diagram exhibiting* a Sm A-Sm C-Sm *F* point

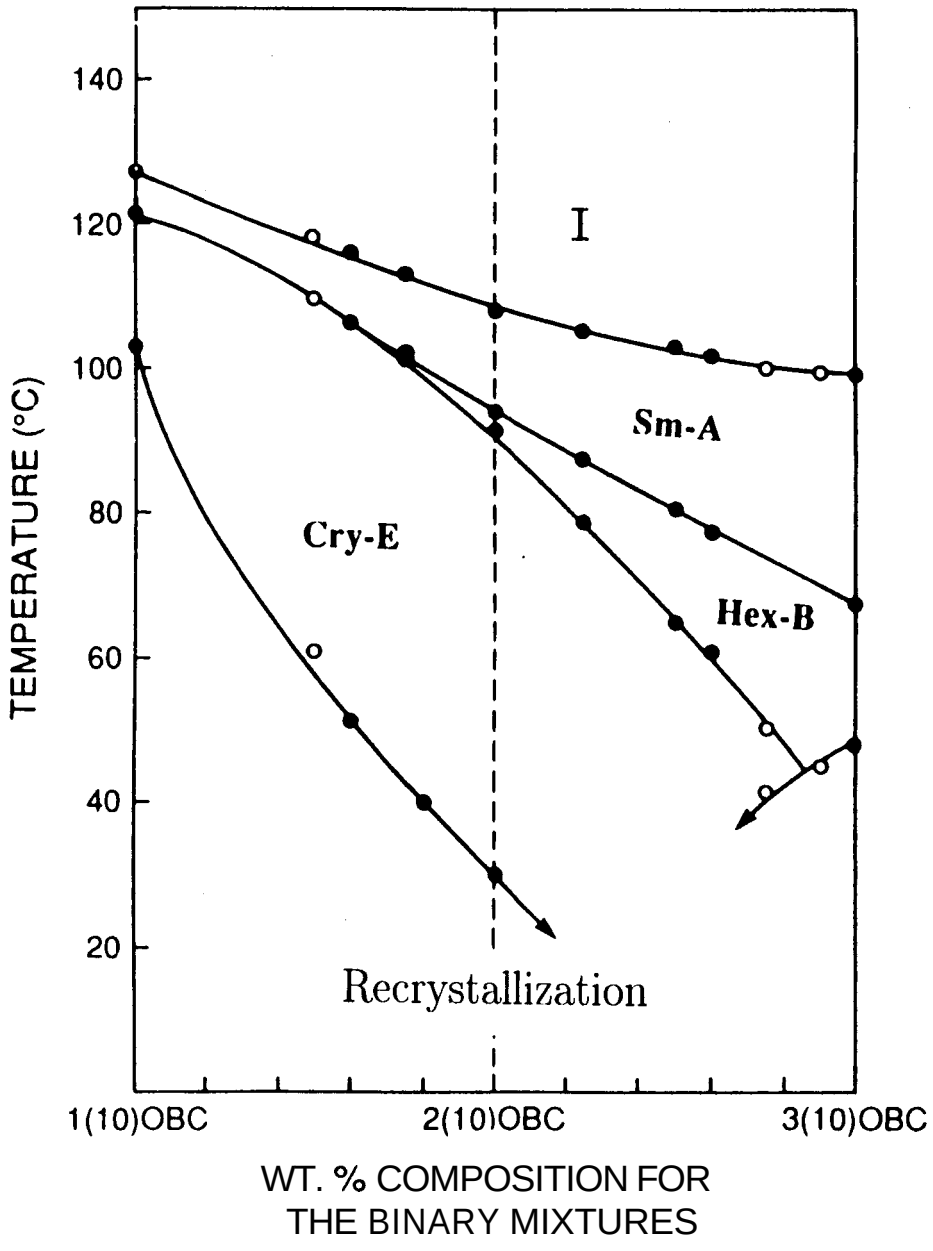

Figure 2.8: Temperature-concentration phase diagram for 1(10)-2(10)OBC and 2(10)-3(10)OBC binary mixtures showing a Sm A-hex B-Cry E meeting point. (From Ref. 13).

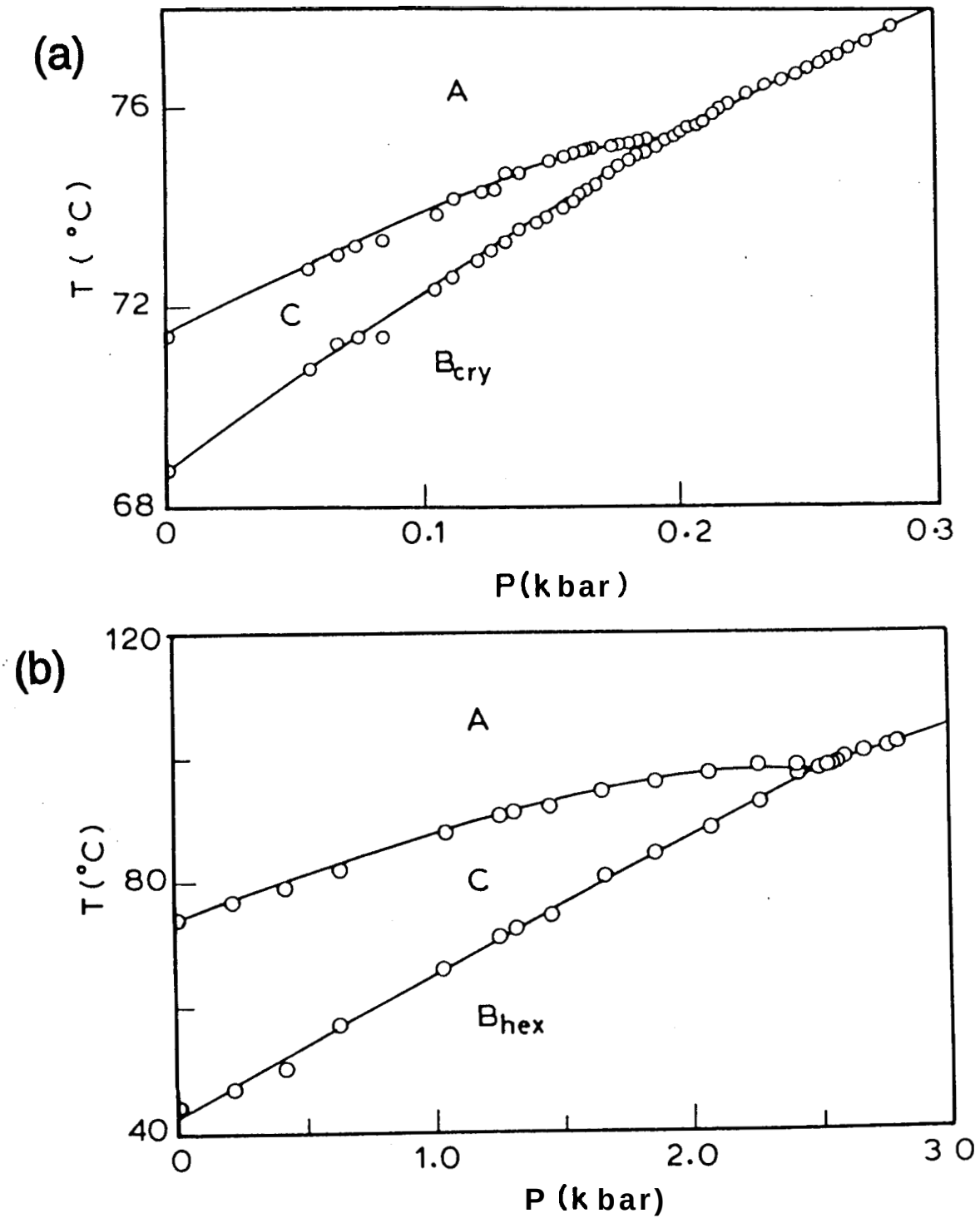

Figure 2.9: The pressure-temperature diagram for (a) 70.7 and (b) 50 mol% of 5OPDOB and 7OPDOB exhibiting Sm **A-Sm** C-Cry B and Sm A-Sm C-hex B meeting points. (From Ref.14).

Phase diagram *exhi*biting a Sm A-Sm C-Sm F point

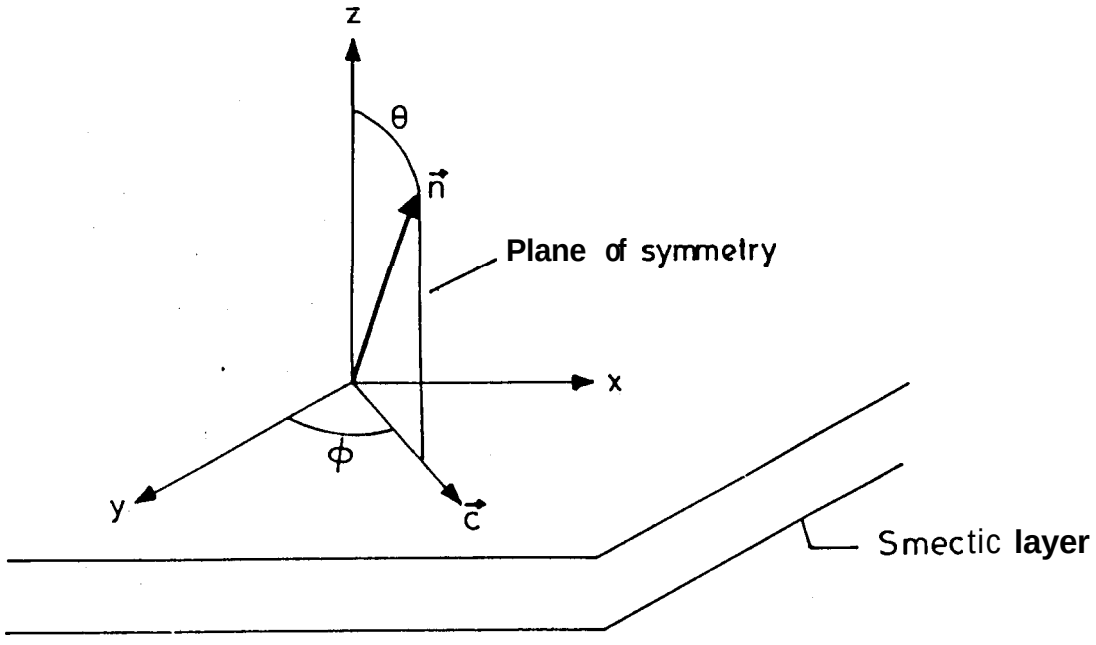

Figure 2.10: Geometry of the smectic C phase.

results Lien and Huang[16] proposed that a cross-over from second order to first order Sm A-Sm C transition may occur when the temperature range of Sm A phase becomes quite small. Later, Liu et al.,[17] argued that the strength of the transverse dipole moment of the constituent molecules has a strong effect on the nature of the Sm A-Sm C transition and hence the transition may not become first order by reducing the temperature range of Sm A phase alone. However, recent studies[18] performed in our laboratory on a homologues series of compounds (terephthal-bis-alkylaniline or TBnA) showed that a substance having a weak transverse dipole moment can still exhibit a first-order Sm A-Sm C transition provided the temperature range of Sm A phase is very small. As a consequence a cross over from a first order to second order transition was observed by just increasing the temperature range of the Sm A phase alone.

- As mentioned earlier,[7] the existence of finite molecular tilt in the Sm C phase gives rise to an induced BOO although of a very small amplitude. Thus both Sm C and Sm F phases have the same symmetry. An important consequence of this is that the Sm C phase transforms to Sm F either through a first order transition or evolves continuously without a phase transition. The latter case is analogous to the transformation between gaseous and liquid phases beyond the critical point.

- The Sm A-Srn F transition can be expected to be a first order one as two different types of symmetries are broken at this transition.

In this chapter we present the experimental studies on a phase diagram exhibit-

Phase diagram exhibiting a *Sm A-Sm C-Sm F* point

ing meeting points of three phases, viz., Sm A, Sm F and Sm C.

2.2 Experimental

Materials Used

The compounds used are terephthal - bis - butylaniline (TBBA)[19] and n - (4 - n - nonyloxy benzylidene) - 4′ - n - butylaniline (90.4) whose structural formulae and transition temperatures are given in Table 2.1.

Sample preparation

The required amount of the materials (90.4 and TBBA) are weighed using a Perkin-Elmer AD2 microbalance with a relative precision of $\pm 1\mu g$. Mixing is done by keeping the sample with a coverslip on a preheated oven, heated to a temperature much above the melting point of both the compounds. A small amount of the sample on a clean glass slide, covered with a coverslip was kept inside a programmable hot stage (Mettler FP82) in conjunction with a polarising optical microscope (Leitz-Orthoplan). Sample temperature was varied slowly at rate of $0.1^{o}C/min$ and the transition temperature was determined by observing the textural changes. The sharpness of the transition temperature determines the purity and homogeneity of the mixture.

Phase diagram exhibiting a Sm A-Sm C-Sm F point

90.4

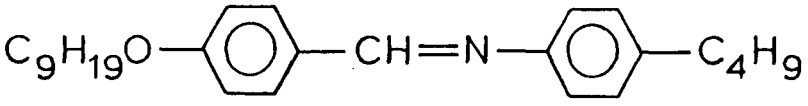

n-(4-n-nonyloxybenzylidene)-4-n-butylaniline

Isotropic	⟶	Sm A	⟶	Sm F	⟶	Cry G
	81.5		G8.8		−66.5	

TBBA

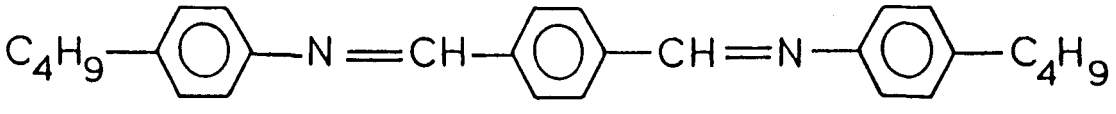

tetrephthal-bis-butylaniline

Isotropic	⟶	N	⟶	Sm A	⟶	Sm C	⟶	Cry G
	236.5		198.3		172.5		144.1	

Table 2.1: Structural formulae and transition temperatures (in °C) of 90.4 & TBBA.

Phase diagram exhibiting a Sm A-Sm C-Sm F point

2.2.1 X-ray Studies

X-ray diffractometer set up

In the initial stages of this work X-ray diffraction experiments were carried out using a scintillation counter as the detector. Later an in situ magnet heater and a position sensitive detector (PSD) were added to the setup. The advantage of using PSD over that of the scintillation counter is that it requires lesser exposure time and allows sirnultaneous scanning over a wide range of scattering angles. Since PSD has been used for most of the experiments a detailed description of it is given below.

X-ray Generator and Monochromator

Figure 2.11 sliows a scliematic view of tlie scattering geometry used in tlie experiments. A conventional X-ray generator (Enraf Nonius, model 583) with a fine focus tube (Philips PW 2213/20 copper anode) was used. The tube was generally operated at 40 kV and 26 mA. The maximum operating conditions of the tube arc 50 kV, 26 mA. But increasing the operating voltage beyond 40kV increases the background radiation and does not really help in getting better X-ray intensity. The beam from the X-ray tube enters the monochromator after passing through a short vacuum path. The monochromator input slits were kept wide open to avoid spurious trimming of the incoming beam. A bent Ge monochromator cut for $(10\bar{1}1)$ reflections was used in the Johansson geometry. The Ge crystal was oriented to select the characteristic CuK_α radiations($\lambda = 1.54051\mathring{A}$). The monochromator exit slits were trimmed to eliminate the $K_{\alpha 2}$ rays so that

Phase *diagram* exhibiting a Sm A-Sm C-Sm *F* point

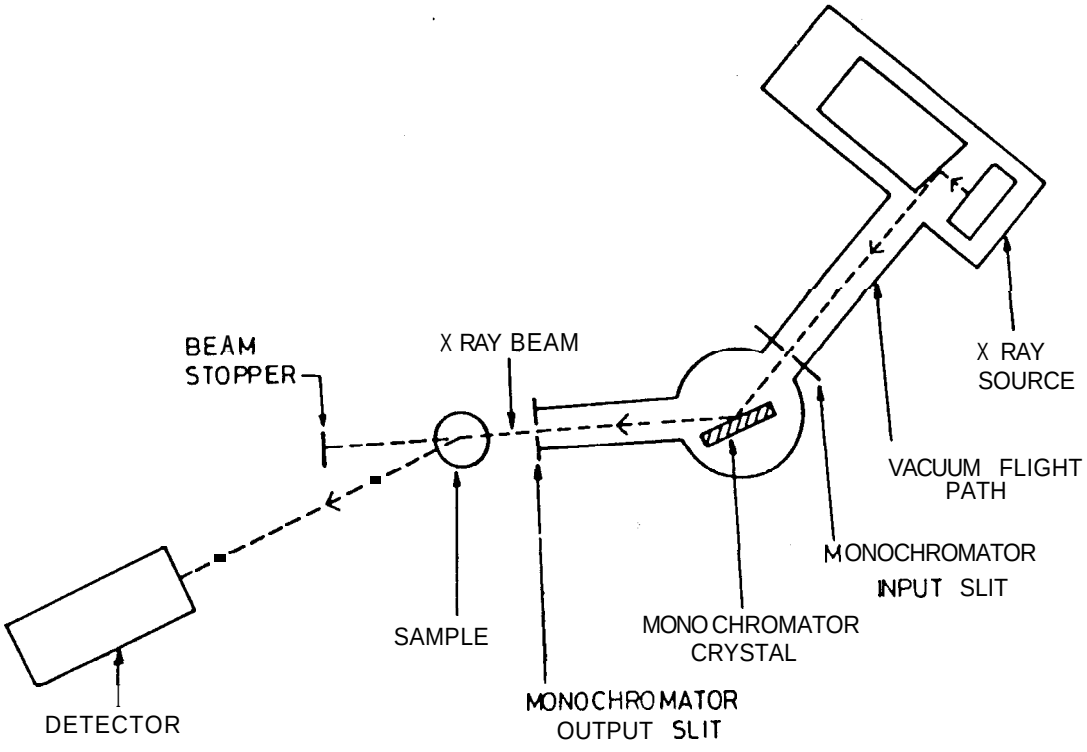

Figure 2.11: Schematic diagram of the X-ray diffraction set up. The detector is either a scintillation counter or a position sensitive detector depending on the set up used.

only $K_{\alpha 1}$ rays emerge from the monochromator. These rays get focussed on the circumference of the Guinier circle. The detector lies on the circumference of the Guinier circle. Details of the detector used is given in a later section.

Sample holder and heater design

Figure 2.12a shows a schematic diagram of the sample holder. The sample holder is made of a copper rod. A narrow bore was drilled along the axis from the top end of the rod to hold 0.5mm Lindemann capillary containing the liquid crystalline sample. The bore was about ~0.6mm in diameter and 12mm in length. A pair of slots are cut on the rod along the length diametrically opposite to each other. These slots serve as tlie entrance and exit slits for the X-ray beams. The edges of the exit slit are tapered so as to have a conical angle of about 30°. This sample holder is inserted into a cavity provided in a small rectangular copper block which also has got entrance and exit slots (see figure 2.12b). There are two screws threaded through the body of this rectangular copper block which help the sample holder windows to align properly with respect to the two slots of tlie block. This is facilitated by means of a matching groove rnade along the axis of the sample holder. These screws also help in firmly anchoring the sample holder to tlie copper block. To the entrance slit of the block, a hylurn lid with a mylar window (to let the incoming X-ray beam) is attached. The mylar window also helps in visual observation and additionally in preventing air draughts.

Figure **2.13** shows sectional view of the heater assembly. It consists of a thick rectangular copper block having a slot at the centre along the breadth to house

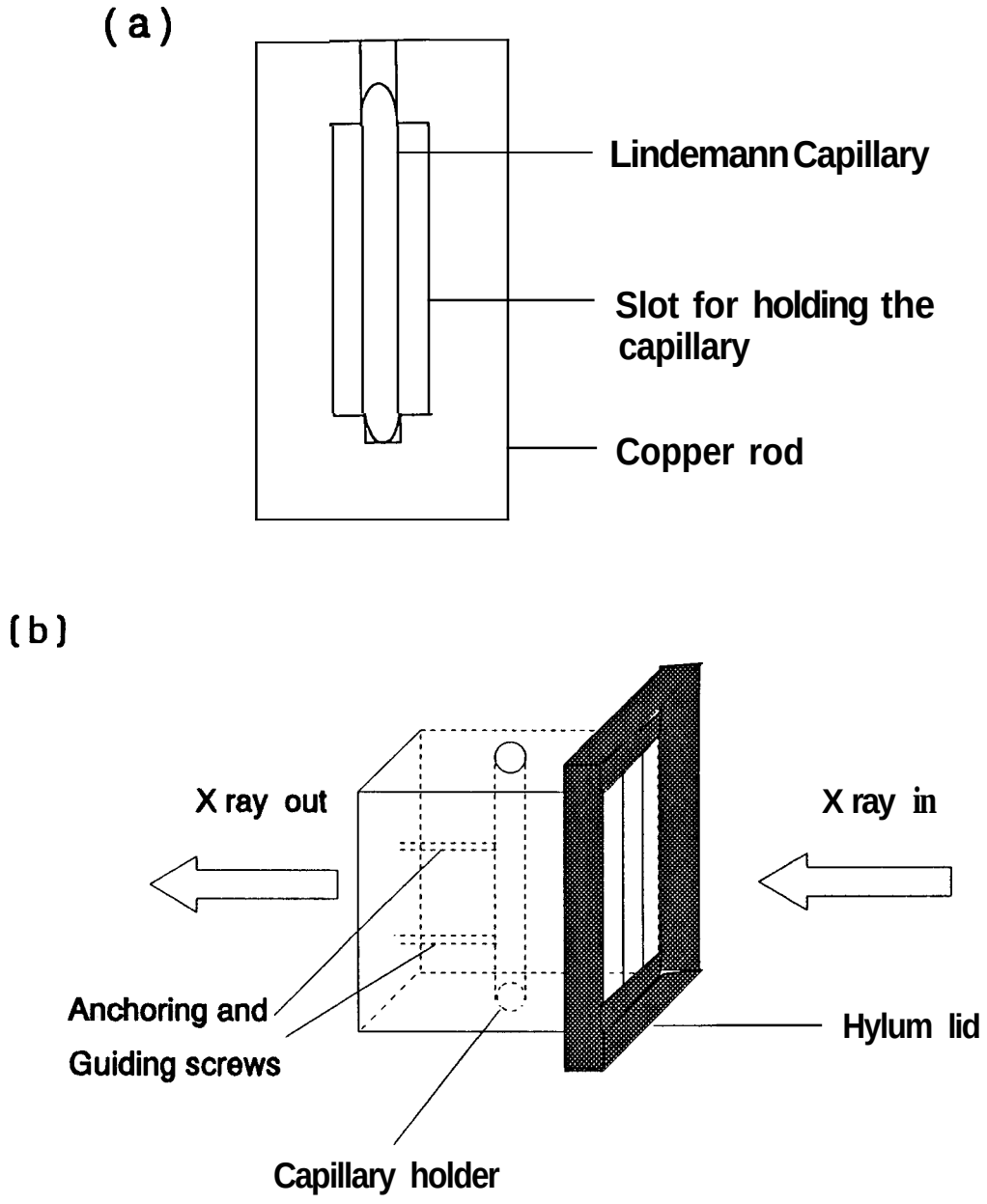

Figure 2.12: A cross-sectional view of the (a) sample holder & (b) sample holder with mount.

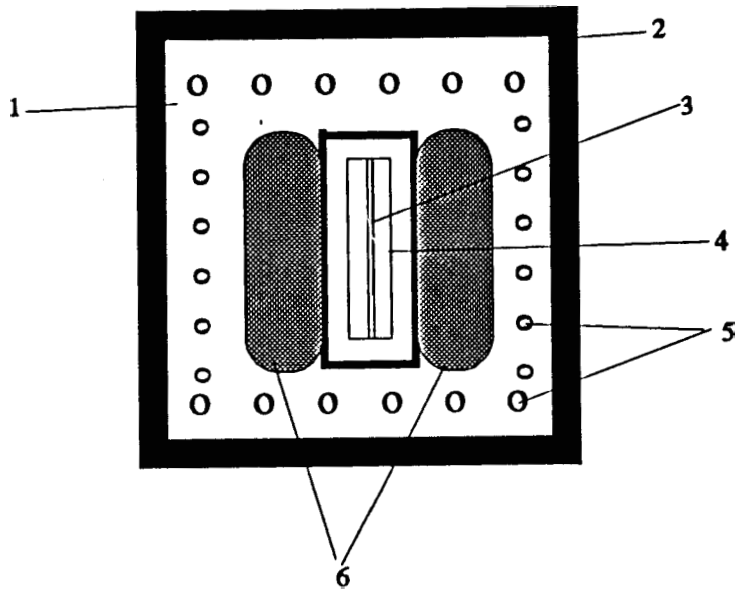

1. Outside Copper Block
2. Hylum Sheeth
3. Sample Capillary
4. Capillary Holder
5. Heater Wires
6. Samarium Cobalt Magnets

Figure 2.13: Cross-sectional view of the heater assembly.

the sample holder. The dimensions are so chosen that the sample holder-inserted in the rectangular copper block fits exactly into the lieatcr. There are cavities present on either side of the sample holder-slot to keep high field strength rare earth ($SmCo_5$) magnets. These are circular (of diameter ~25mm) in shape arid provide a magnetic field of 0.8T. One of the junctions of the chromel-alumel thermocouple sheathed in a ceramic tube is inserted through a hole drilled from the top of the heater. The junction of the thermocouple was positioned with an epoxy so that it sits in close proximity to the sample. Thermofoil(MINCO) heater wrapped around the copper block facilitates temperature variation of tlie heater, or in otherwords that of the sample. The input power to the thermofoil was supplied using a high stability programmable DC power supply (Helwett Packard, Model 6038A). The copper block is covered with insulating materials, namely, asbestos sheets and an hylum block. This minimizes the loss of heat due to radiation. The exit window is covered with a thin mylar sheet which along with the mylar window of the entrance slit helps in preventing the air draughts.

The output of the chromel-alumel thermocouple was fed to a high resolution, low drift voltmeter (Keithley nanovoltmeter Model 181). To obtain the true sample temperature the thermocouple was calibrated using standard substances exhibiting sharp phase transitions. Samples were taken in 0.5mm Lindemann capillaries. A light transmission technique was used to monitor the transitions. Light from a laser bearn was made to fall on the sample and the transmitted intensity was collected using a photodiode, the output of which was recorded on a multichannel recorder. The temperature at which there is an abrupt change in intensity is taken as the transition temperature in milli-

volts(mV). The absolute transition temperatures were determined(in °C) using polarizing microscope (Leitz-Orthoplan) in conjunction with a programmable hot stage (Mettler FP82). Transition temperature in °C and the therrno emf in mV obtained in tliis way for various compounds are tabulated in Table 2.2 and plotted in figure 2.14. For numerical conversion between the thermo-emf(in mV) and the temperature(°C), the data was fitted to a fifth degree polynomial,

$$T = a_o + a_1 \times mV + a_2 \times mV^2 + a_3 \times mV^3 + a_4 \times mV^4 + a_5 \times mV^5 \quad (2.2)$$

where, a,, a_1, a_2, a_3, a_4 and a_5 are constants, mV is the thermoemf in millivolts. From the figure 2.14 it is evident that the polynomial fits the data extremely well and can be used to convert the thermocouple output to sample temperature.

Position Sensitive Detector (PSD)

Figure 2.15 shows block diagram of the X-ray detector set up. The linear Position Sensitive Detector used (mBraun, OED50s) is simply a gas filled ion chamber capable of furnishing information about the place of incidence of the incoming quanta. The physics of operation is like that of a classical How proportional counter. A brief description of the PSD and its principle of operation is given below.

The counting tube has a two-walled construction. The outer stainless steel case functions as a shield as well as a pressure seal. The inner aluminium case electrically isolated from the outer case contains a high-resistance carbon coated quartz wire ($25.4\mu m$ diameter and electrical resistance $\rho = 8k\Omega/\text{mm}$). It is tliis wire that is essential for extracting out positional information of the diffracted

Phase diagram exhibiting a Sm A-Sm C-Sm F point

Table 2.2: Thermocouple calibration of the heater. Materials used and the transition temperatures.

Compound	Transition temperature (°C) (Mettler)	Thermo emf (mV) (heater)	Fit values
8CB	40.05	1.6321	40.05
8OCB	80.05	3.3041	80.04
CBOOA	107.3	4.4494	107.3
(p-ethoxyphenylazo) -phenylheptonoate	118.6	4.9217	118.59
PAP	166.95	6.8922	**166.94**
4-n-alkoxybenzylidene-N-(phenylazo)-aniline	201.25	8.2445	201.25

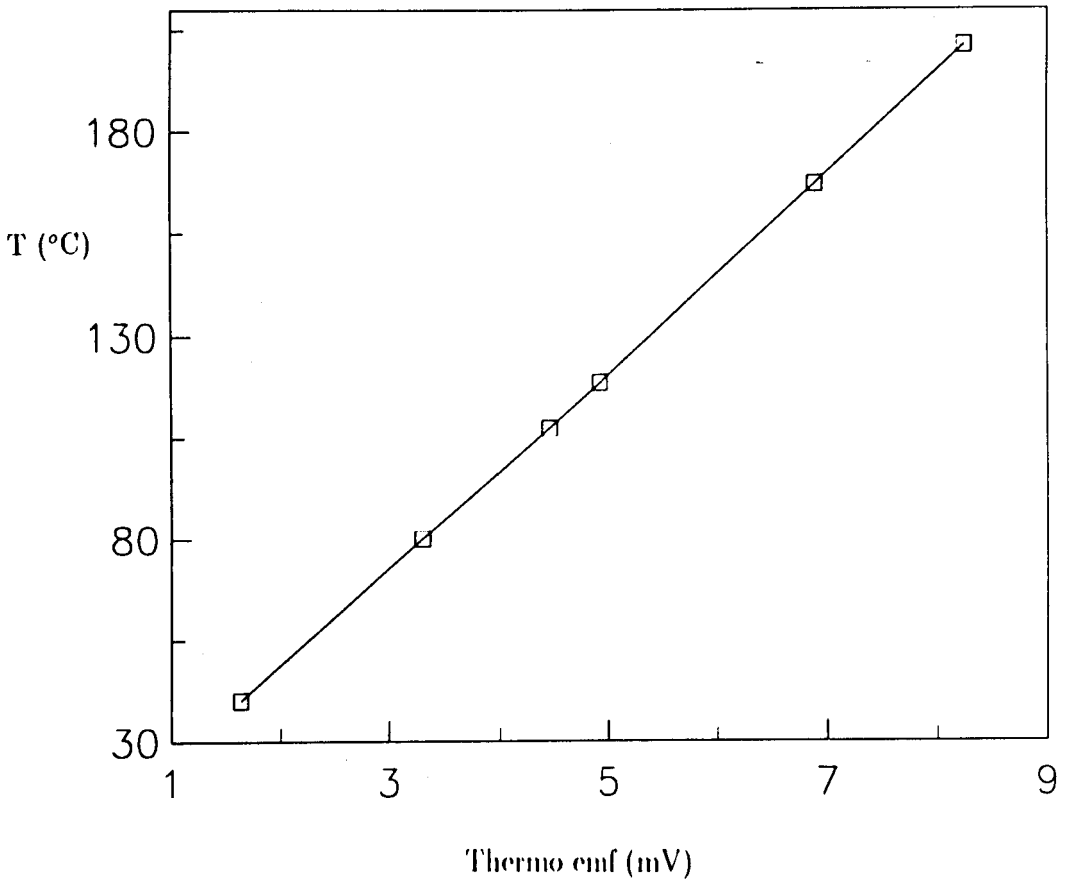

Figure 2.14: Thermocouple calibration curve for the X-ray heater. □ represent the data points and solid line is a fit to a 5th degree polynomial.

Phase *diagram* exhibiting a *Sm A-Sm* C-Sm *F* point

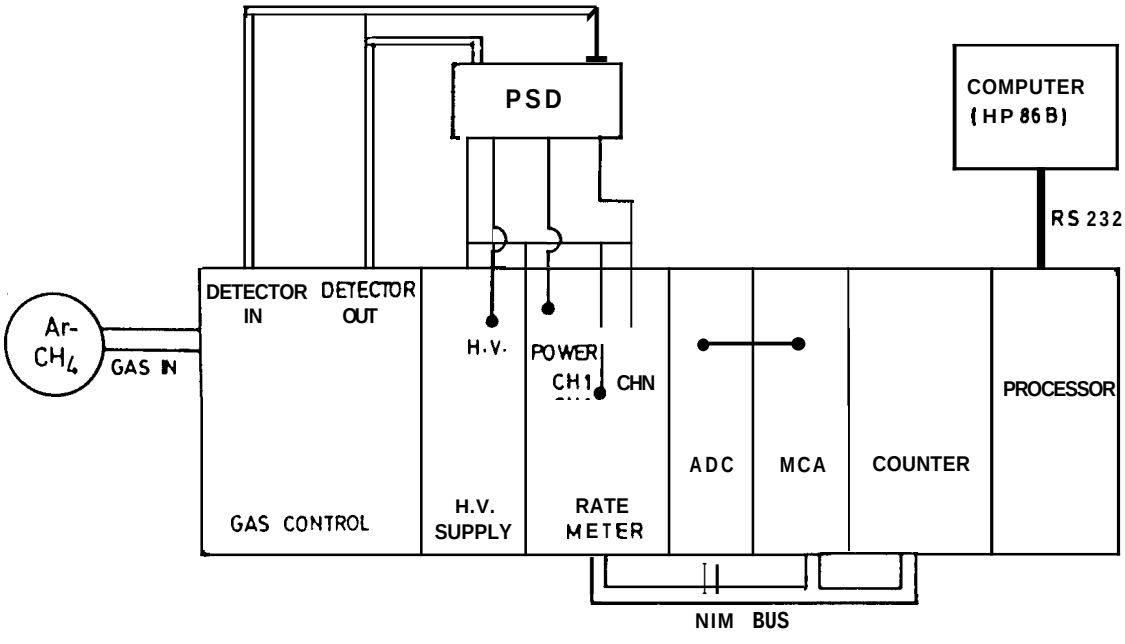

Figure 2.15: Block diagram of the X-ray detector setup.

beam. The ends of the wire are directly connected to the FET-input of the pre-amplifier circuit. To filter out any extraneous light or dust particles entering the chamber, the entrance window of the detector is covered by a thin (0.4mm) beryllium foil with a high degree of transparency to X-rays.

To create electron avalanche, the basis of gas proportional counters, argon-methane (90% argon and methane 10%) is used as counter gas. In order to increase the quantum efficiency, the counter is operated at a pressure of $\sim$ 11 bar and the flow is maintained at a uniform rate of $\sim$0.5 millilitre/hour. The signal voltage of the preamplifier (mounted at the back of the detector) is further processed using an amplifier, energy discriminator and a time-to-amplitude converter. Position coordinates are digitised by a 2K Multichannel Analyser. An integrated computer handled initiation and accumulation of scans, on-line graphic presentation of the data, output of the data to serial port for communication with the main computer, etc. The stored data were transferred to the main computer (HP 86B) for further analysis and data reduction. To calculate the Bragg angle θ from the channel information, the following expression was used.

$$\theta = -0.5 \times \tan^{-1}\left[(y - (CHC - CH) \times INKR)/r\right] \qquad (2.3)$$

where, CHC is the central channel number, CH the channel number corresponding to the diffracted beam from the sample, r the distance of the sample from the counter (in mm) and INKR is the reciprocal of the number of channels per mm, y any shift (in mm) of the central channel with respect to the main beam. The layer spacing d corresponding to ,this Bragg angle is calculated using the

Phase diagram exhibiting a Sm A-Sm C-Sm F point

formula

$$d = \frac{\lambda}{2 \sin 8} \tag{2.4}$$

Wavevector resolution

The wavevector spread or the resolution(dq) in the equatorial direction is calculated from the equation, $dq = \frac{4\pi}{\lambda} \cos\theta d\theta$. For a typical scattering angle of 1.1^{o}, dq = 1 x $10^{-3}\mathring{A}^{-1}$. In other words this set up permits us to resolve two peaks whose minimum separation in q space is 1 x $10^{-3}\mathring{A}^{-1}$. The precision in the determination of wavevector(q) itself was 2 x $10^{-4}\mathring{A}^{-1}$.

During each measurement, the sample temperature was maintained to a constancy of ± 5 mk. The temperature measuring nanovoltmeter(KEITHLEY 181) was also interfaced to HP86B computer.

Scintillation counter set up

In this set up[20] a quartz monochromator and a scintillation counter were used instead of the Ge monochromator and the position sensitive detector set up described above. The precision in the determination wavevector is $2 \times 10^{-4}\mathring{A}^{-1}$ while in the equatorial direction it is $1.42 \times 10^{-3}\mathring{A}^{-1}$.

2.3 Results and Discussion

The partial temperature-concentration(T-X) phase diagram (X is the weight fraction of '30.4 in the mixture) obtained by optical microscopy and X-ray studies is as shown in the figure 2.16. 90.4 exhibits a direct transition from Sm **A**

Phase diagram *exhi*biting a Sm A-Sm C-Sm F point

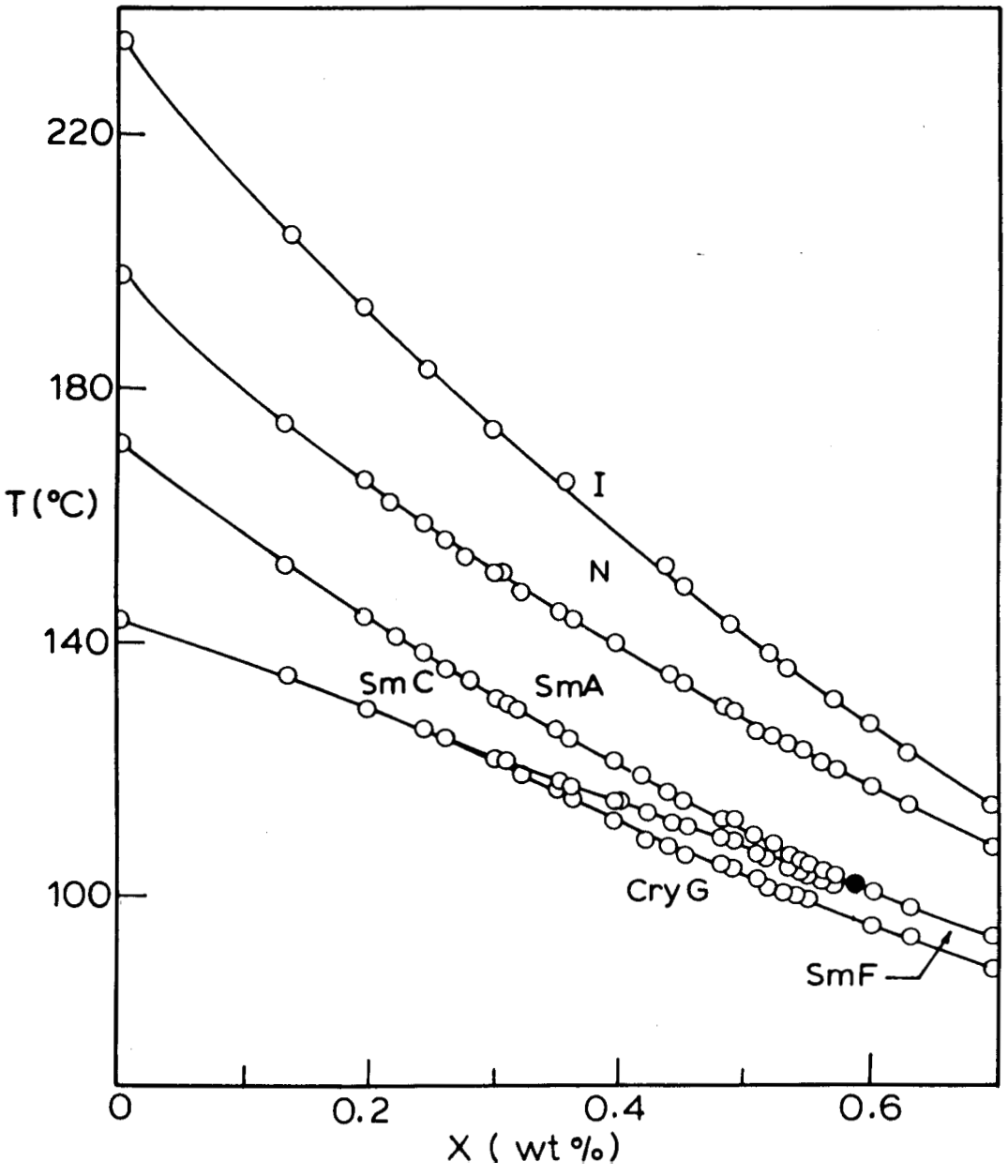

Figure 2.16: Partial temperature-concentration phase diagram for varying weight fraction (X) of 90.4 in TBBA. The solid lines are guides to the eye. The Sm A-Sm C-Sm F point is denoted by the solid circle.

to Sm F phase while TBBA exhibits the sequence Sm A⟶Sm C⟶Cry G. The latter scqucnce is retained for concentrations upto X≃0.28. When X>0.28, the Sm F phase appears between the Sm C and Cry G phases. With increasing concentration of 90.4 in TBBA, the temperature range of the Sm F phase increases at the expense of Sm C phase range. Finally, for X>0.585 the Sm C phase ceases to exist resulting in a Sm A-Sm C-Sm F meeting point. Mixtures rich in 90.4, i.e., X>0.585, show a direct transition from Sm A to Sm F phase. Figure 2.17 shows the topology of the phase diagram near tlie Sm A-Sm C-Sm F meeting point on an enlarged scale.

With a view to characterizing the nature of this point, X-ray experiments have been done for eleven different concentrations in the vicinity of the meeting point. Before discussing our results, it may be relevant to recall reports in literature on the nature of the transition in the two constituent compounds. Magnetic birefringence measurements of Rosenblatt et al.,[21] have shown that the Sm A-Sm F transition in 90.4 is strongly first order. This is said to have been confirmed by calorimetric measurements also(C.C.Huang, referred in Ref.21). High-resolution X-ray measurements[22] across the Sm A-Sm C transition of TBBA have shown that it is of second order type.

Figure 2.18 sliows the thermal variation of layer spacing d across Sm A-Sm C transition for X=0.32. The continuous variation in d with temperature, along with a similar variation in the peak intensity of scattering(see figure 2.19) indicates that the transition is second order. The transition continues to be second order with increase in X till X=0.4 (see figures 2.20 & 2.21). But with further

Phase ***diagram*** **exhibiting a** ***Sm*** **A-Sm** ***C-Sm F*** **point**

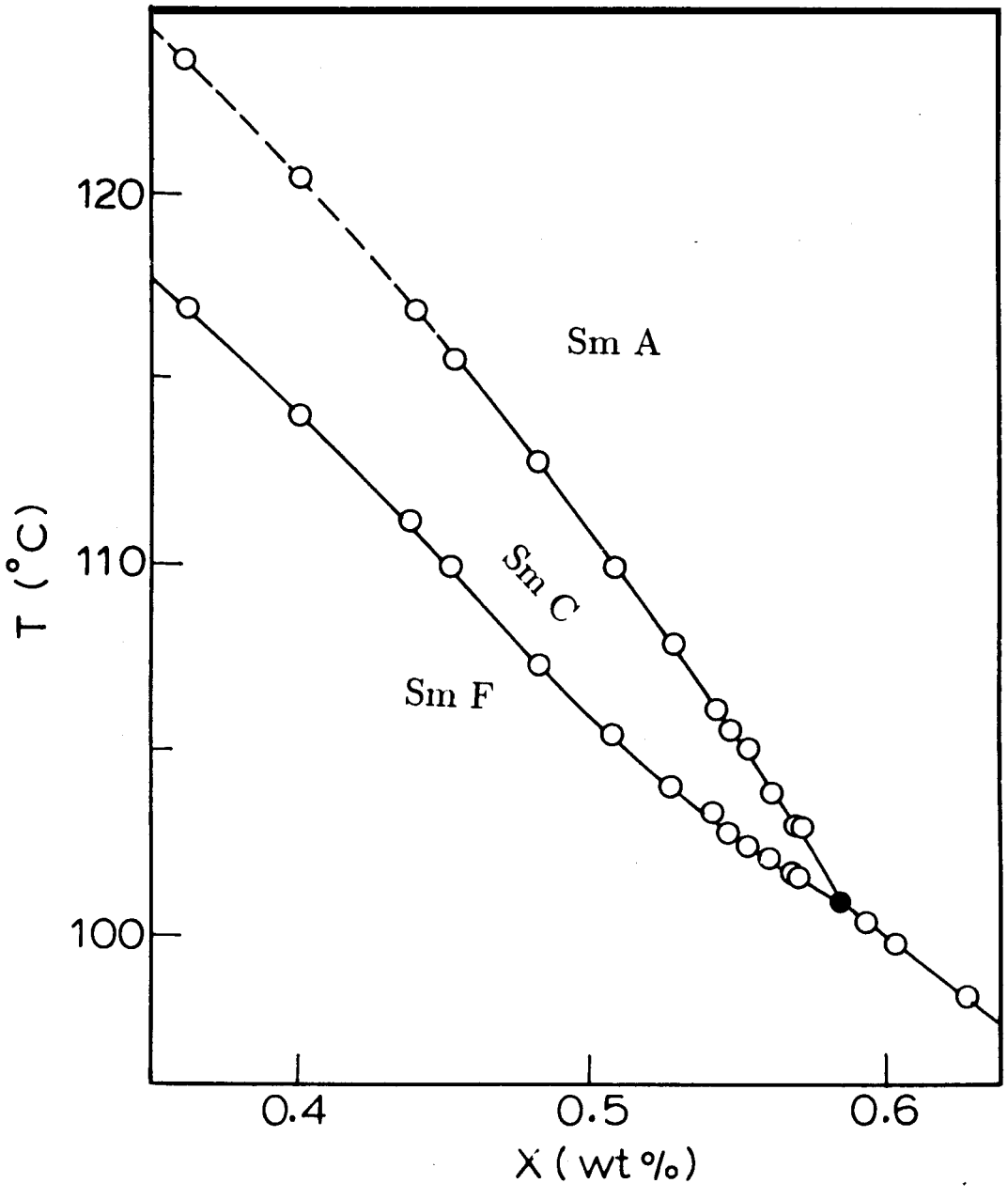

Figure 2.17: Partial temperature-concentration phase diagram near Sm A-Srn C-Sm F meeting point. Sm F-Cry G phase boundary is not shown in this figure.

Phase diagrain exhibiting *a* Sm A-Sin *C-Sm F* point

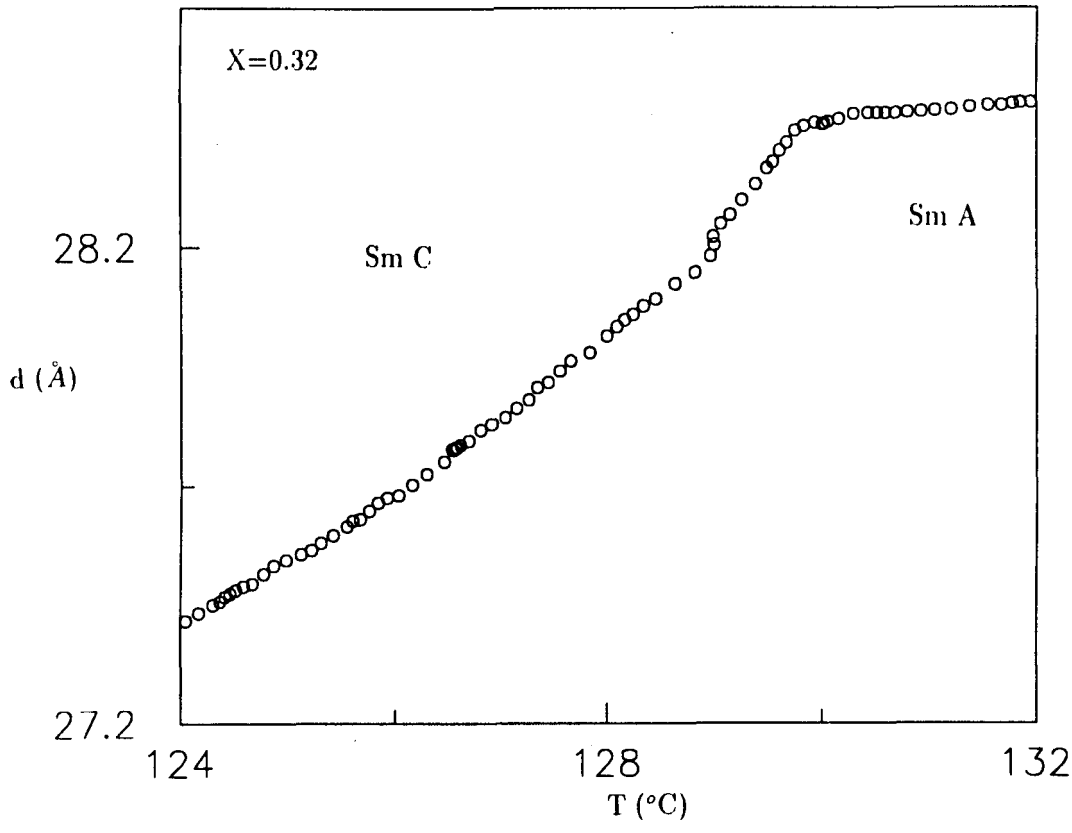

Figure 2.18: Temperature variation of the layerspacing d in the vicinity of Sm A-Sm C transition for X=0.32. The continuous variation in d indicates that the transition is second order.

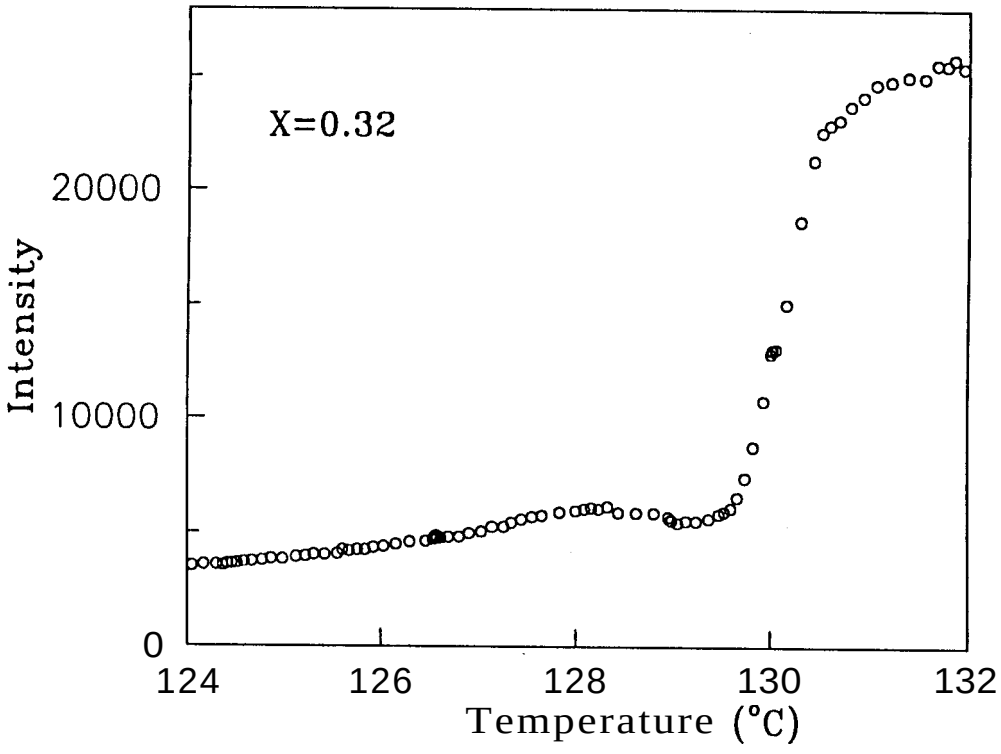

Figure 2.19: Thermal variation of intensity near Sm A-Sm C transition for X=0.32. Note the continuous variation in intensity across the transition.

Phase diagram exhibiting *a* Sm A-Sm *C-Sm F* point

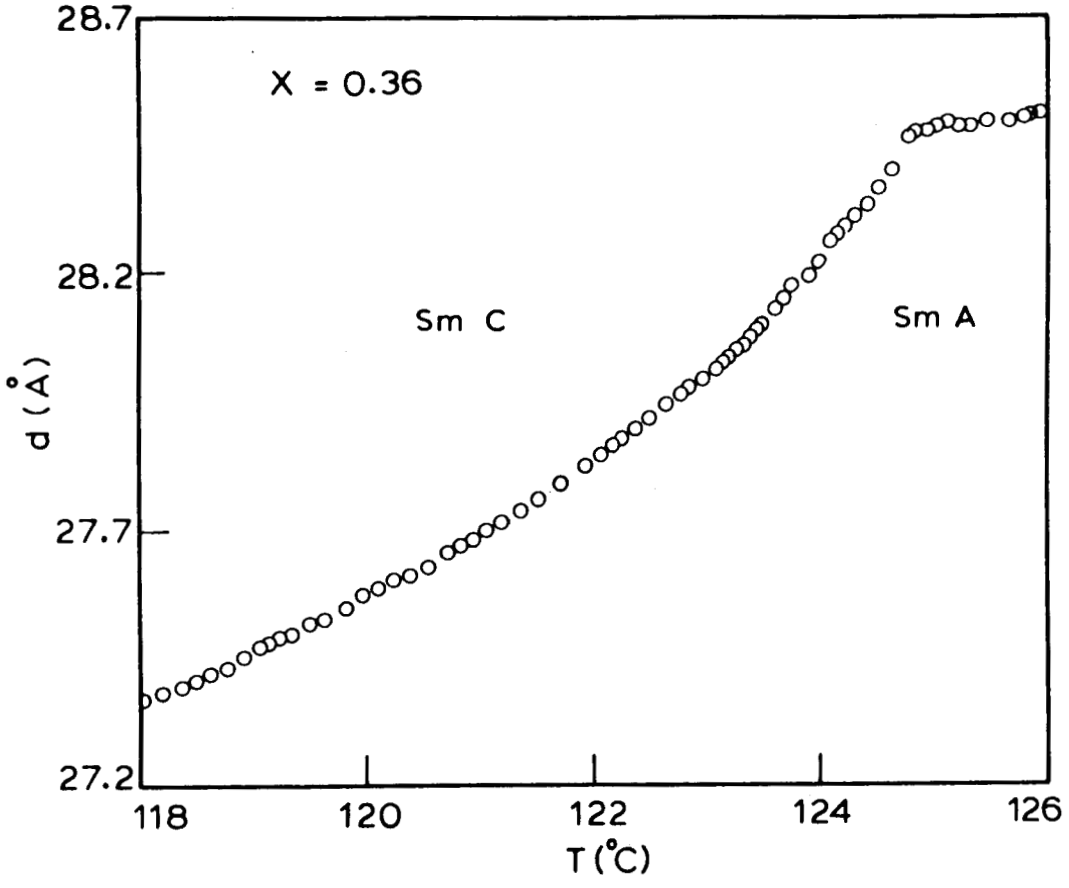

Figure 2.20: Thermal variation of d near Sm A-Sm C transition for X=0.36.

Phase diagram exhibiting a *Sm* **A-Sm** *C-Sm F* point

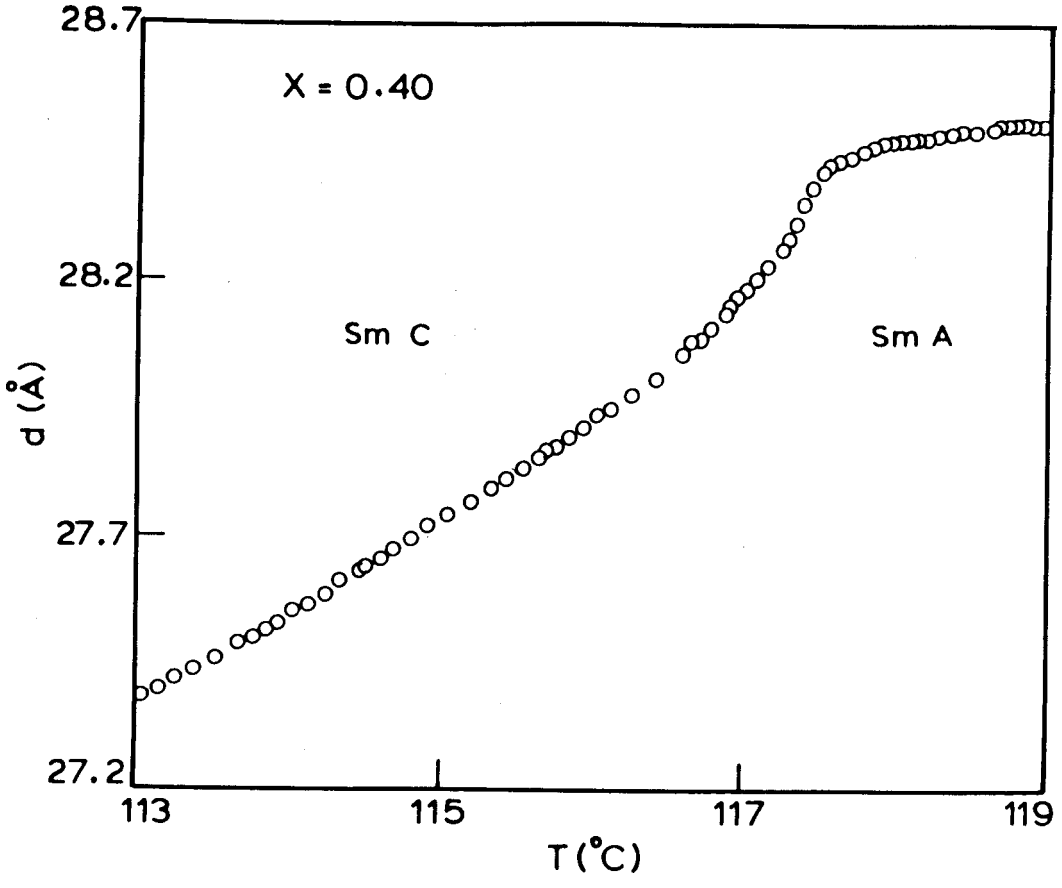

Figure 2.21: Thermal variation **of** d near Sm A-Sm C transition **for** X=0.40.

increase in concentration of 90.4, there is a change in the scenario. For X=0.45 (see figure 2.22) the transition is first order marked by a jump in d accompanied by a two-phase coexistence region wherein the modulations corresponding to both the phases are present, signifying that the transition is first order. In fact, these features are exactly as expected and indeed observed earlier for a first order Sm A-Sm C transition.[18] In addition, the thermal variation of intensity shows a cross-over behaviour confirming that the transition is first order (see Figure 2.23). Figures 2.24 and 2.25 show that Sm A-Srn C transition remains first order for all higher values of X till Sm A-Sm C-Sm F meeting point. The magnitude of the tilt angle, θ, is calculated using the expression,

$$\theta = \cos^{-1}(d_C/d_A) \tag{2.5}$$

where d_C *and* d_A are the layer spacing values in the Sm C and Sm A pliases respectively. The thermal variation tilt angle(θ) close to Sm A-Sm C transition for different concentrations is plotted in the figure 2.26. It is clear that for X $\leq$ 0.4, the tilt angle(θ) goes continuously to zero as for a second order transition, whereas for X$\geq$ 0.45, the tilt angle jumps abruptly to zero indicating a first-order transition. Evidently there is a tricritical point in the concentration range $0.4 \leq X \leq 0.45$.

We have also carried out X-ray experiments on mixtures exhibiting Sm C-Sm F transition. Figure 2.27 shows the thermal variation of d across this transition for X=0.32. The jump in the layer spacing and the presence of two-phase co-existence region confirm that the Sm C-Sm F trarisitiori is of first order type.

Figure 2.28 shows the variation in layer spacing versus temperature for four

Phase diagram exhibiting a Sm A-Sm *C-Sm F* point

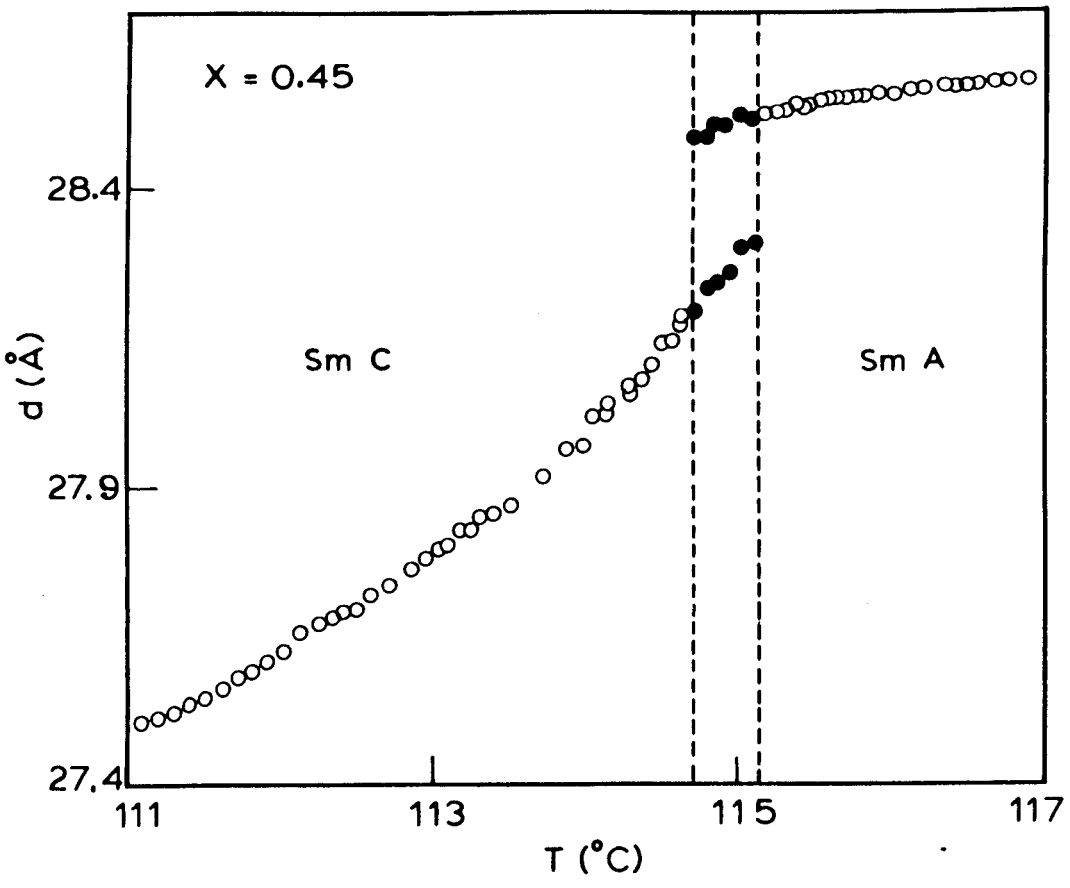

Figure 2.22: Temperature dependence of d near Sm A-Sm C transition for X=0.45. Filled circles represent the data in the two-phase region characteristic of a first order transition.

Phase *diagram* exhibiting a *Sm A-Sm C-Sm F* point

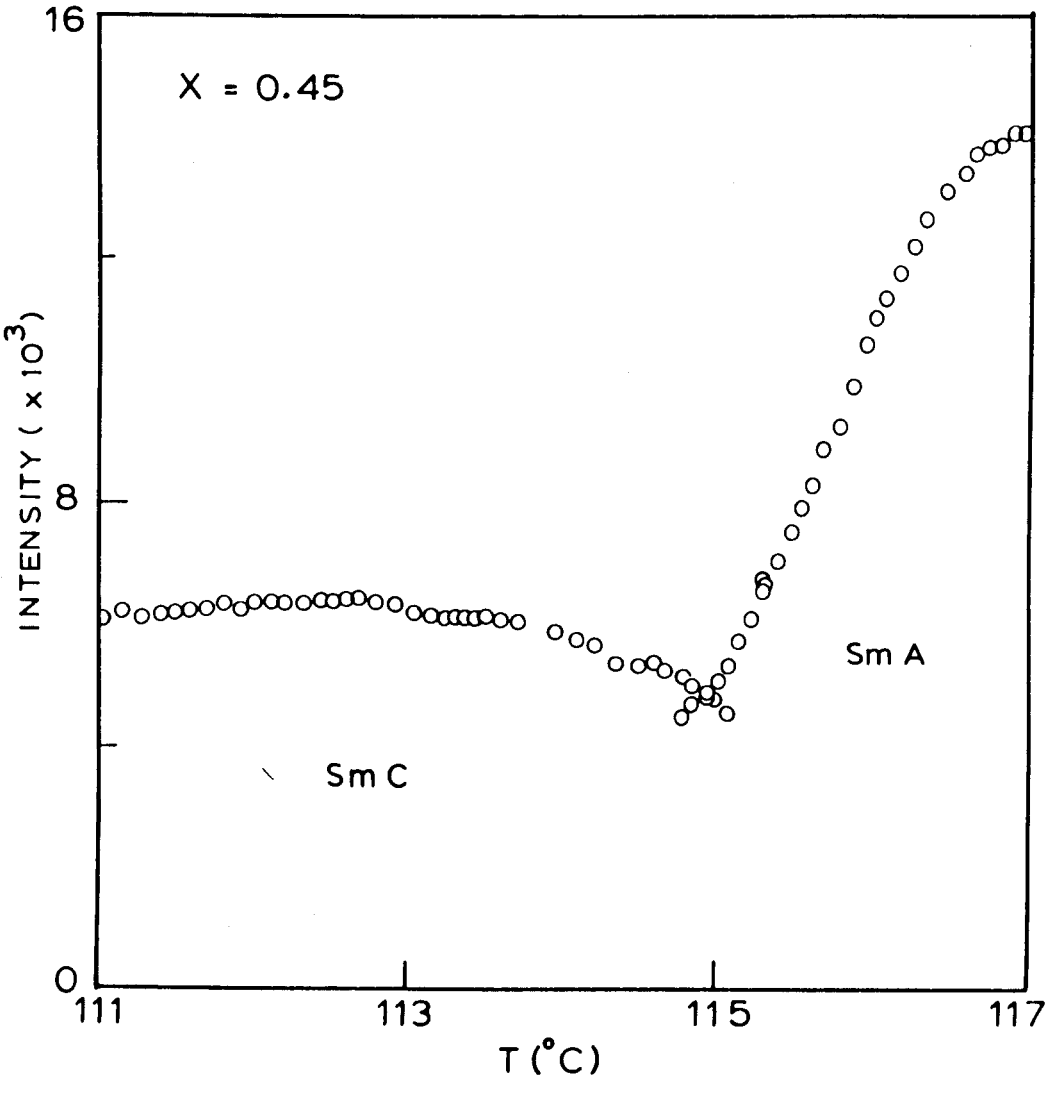

Figure **2.23:** Intensity vs. temperature plot near Sm **A-Sm** C transition for X=0.45. The cross-over behaviour in intensity across the transition supports the first order nature.

Phase *diagram* exhibiting a *Sm A-Sm C-Sm F* point

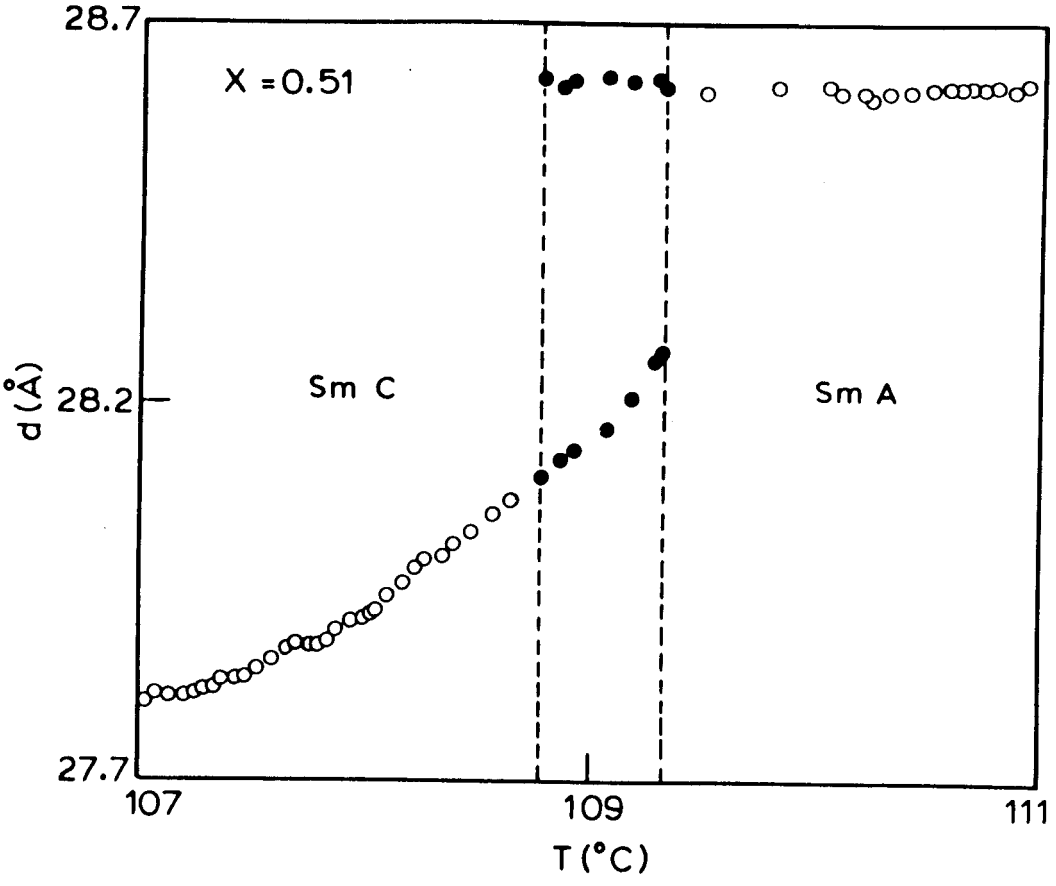

Figure 2.24: *d* vs. T plot near Sm A-Sm C transition for X=0.51.

Phase diagram exhibiting a Sm A-Sm C-Sm F point

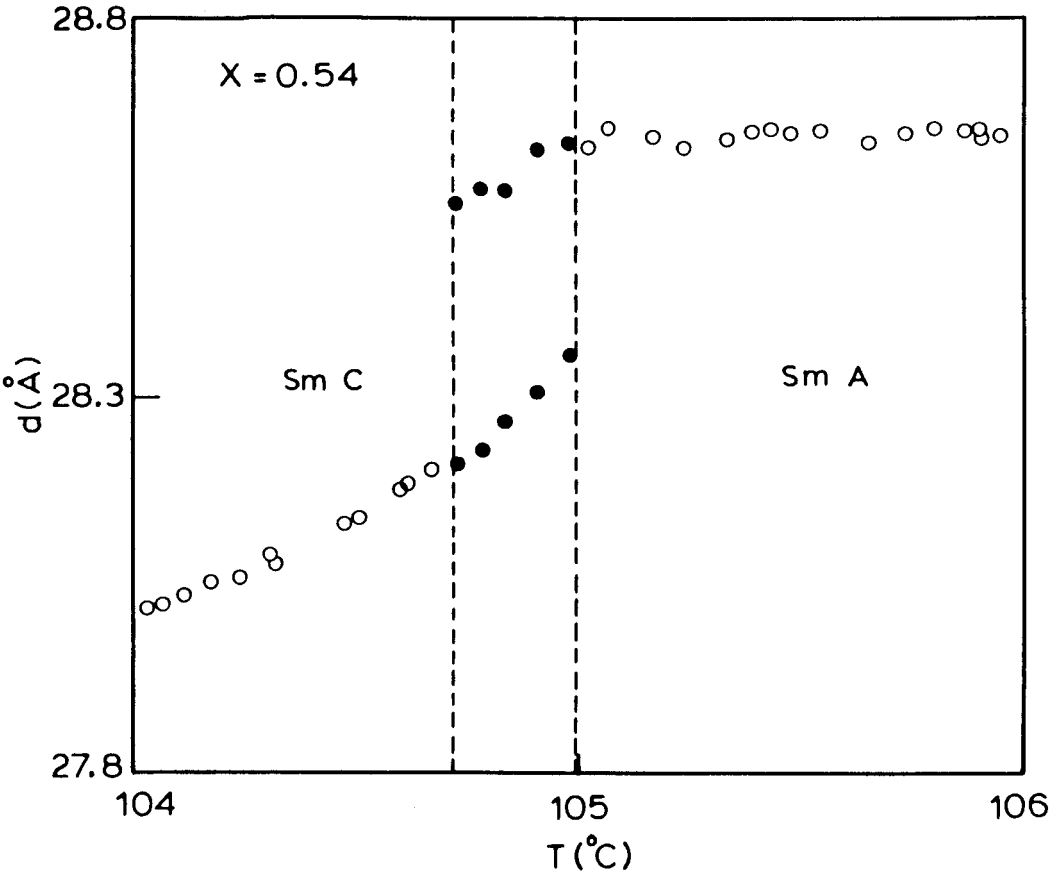

Figure 2.25: d vs. T plot near Sm A-Sm C transition for X=0.54.

Phase diagram exhibiting *a Sm A-Sm C-Srn F* point

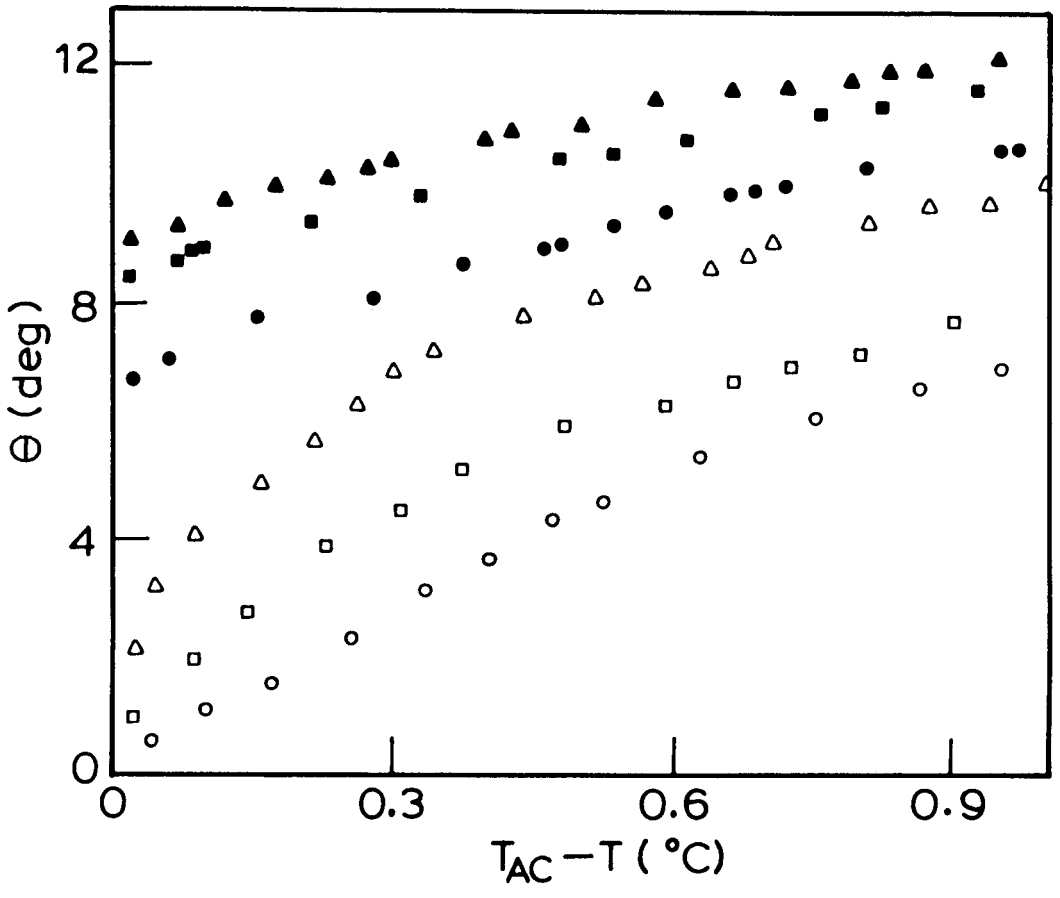

Figure 2.26: Smectic C tilt-angle variation vs. the reduced temperature for X=0.54 (A), 0.51 (■), 0.45 (•), 0.4 (A), 0.36 (□) and 0.32 (o).

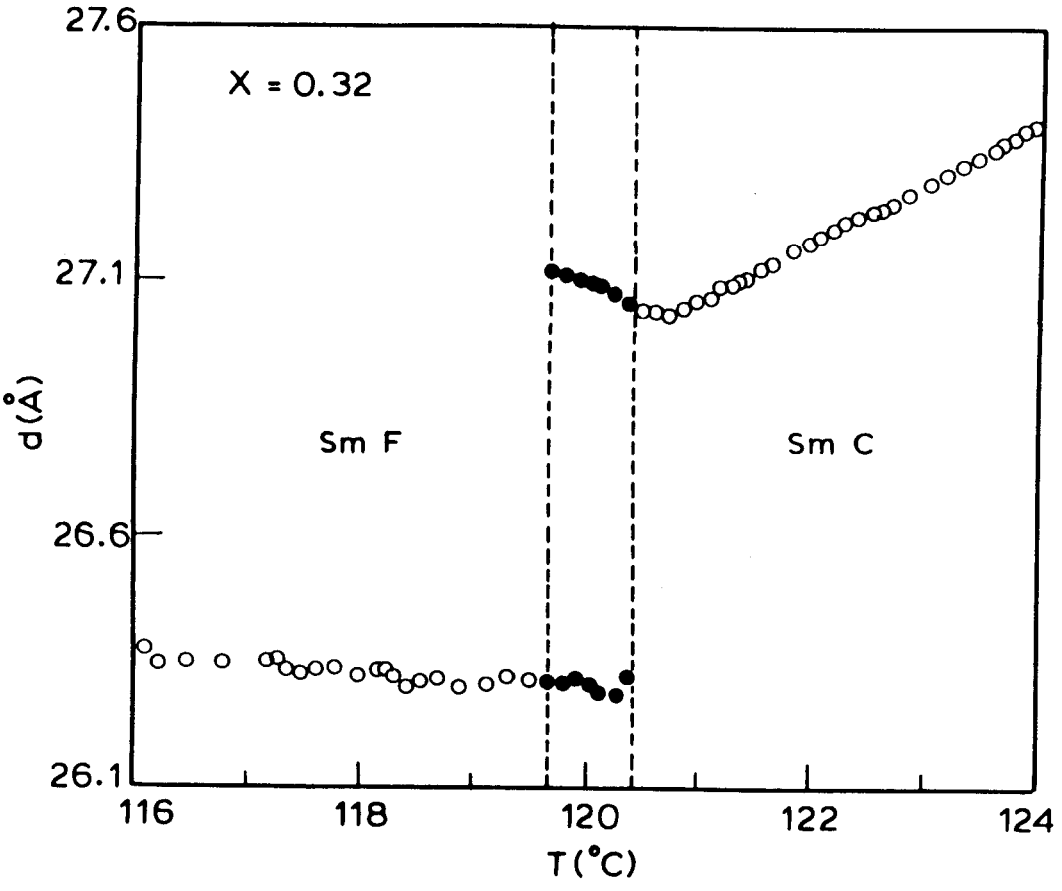

Figure 2.27: Thermal variation **of d** near Sm C-Sm **F transition for** X=0.32. The vertical dashed lines indicate the two-phase region.

Phase *diagram* exhibiting a *Sm A-Sm C-Sm F* point

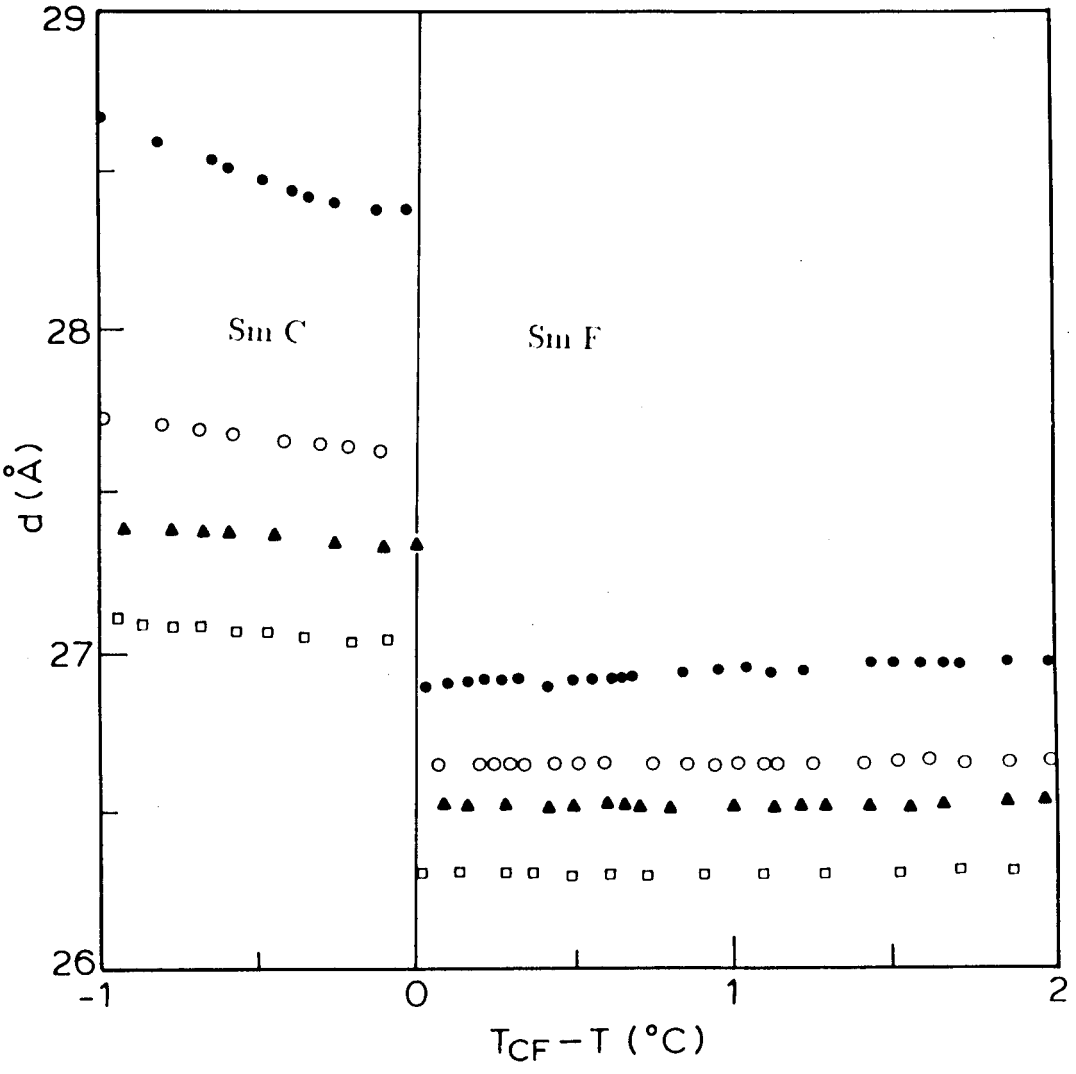

Figure 2.28: Variation of d as a function of the reduced temperature in the vicinity Sm C-Sm F transition for X=0.56 (e), 0.44 (o), 0.36 (A) and 0.32 (□). For the sake of clarity, the data in the two-phase region correspondirig to tlic Sm C phase are not shown.

different concentrations, namely, X=0.32, 0.36, 0.44 and *0.56.* It is clear from the figure 2.28 that Sm C-Sm F transition, marked by the jump in d, is first order for all the mixtures studied. The figure 2.29 shows the jump in layer spacing **(Ad)** across Sm C-Stn F transition versus concentration. Interestingly Ad is observed to increase with increase in tlic temperature range of Sm F phase. Note that the Sm F phase temperature range was found to increase with increase in concentration(X) as shown in the phase diagram (Figures 2.16 and 2.17). A similar trend has been observed[22] across Sm C-Sm F transition exhibited by lower members of Terephthal-bis alkyl aniline (TBnA) series. Benattar et **al.,**[23] also showed similar behaviour for four different homologues (n=10, 13, 15 and 19) of the same TBnA series which exhibit the Sm C-Sm I transition.

Figure 2.30 shows thermal variation of d for X=0.6, a concentration which is close to the Sm A-Sm C-Sm F meeting point. The Sm A-Sm F transition is seen to be first ortlcr marked by tlic jump in d and also by the presence of a two-phase coexistence region.

The results mentioned above show that all the three phase boundaries, namely, Sm A-Sm C, Sm C-Sm F and Sm A-Sm F, are first order near the Sm A-Sm C-Sm F meeting point. Hence tlic Sm A-Sm C-Sm F point, a meeting point of three first ortlcr boundaries, is a *triple point.* This is the first observation of a phase diagram showing a meeting point of Sm A, Sm C and a tilted hexatic phase, namely, Sm F. Another interesting feature of these studies is the observation of a tricritical point on the Sm A-Sm C phase boundary. As mentioned earlier, the Sm A-Sm C transition changes over from second ortlcr

Phase *diagram* exhibiting a. *Sm A-Sm C-Sm F* point

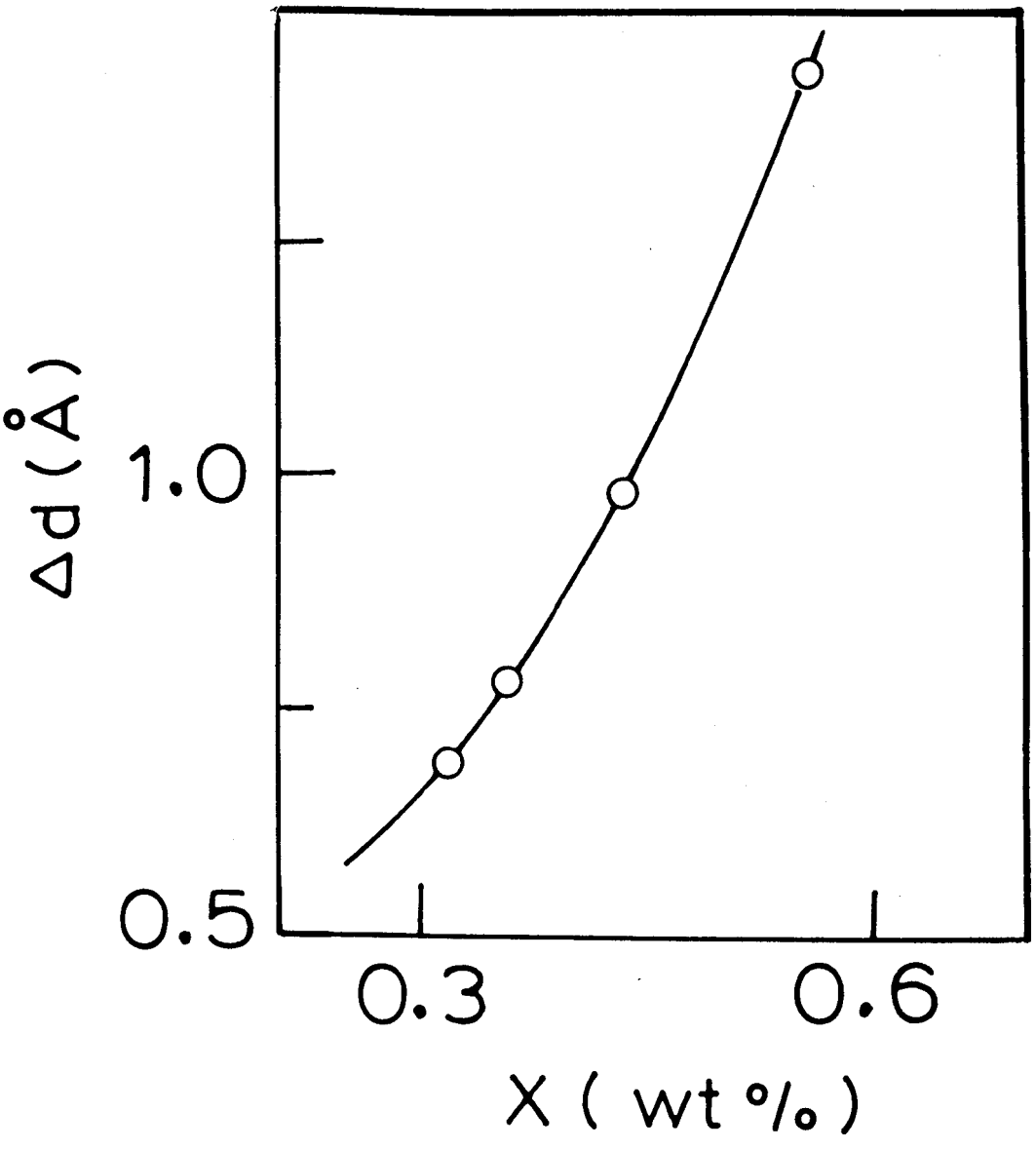

Figure 2.29: Plot showing the jump in d across. Sm C-Sm F transition vs. concentration.

Phase *diagram exhibiting* a *Sm A-Sm C-Sm F point*

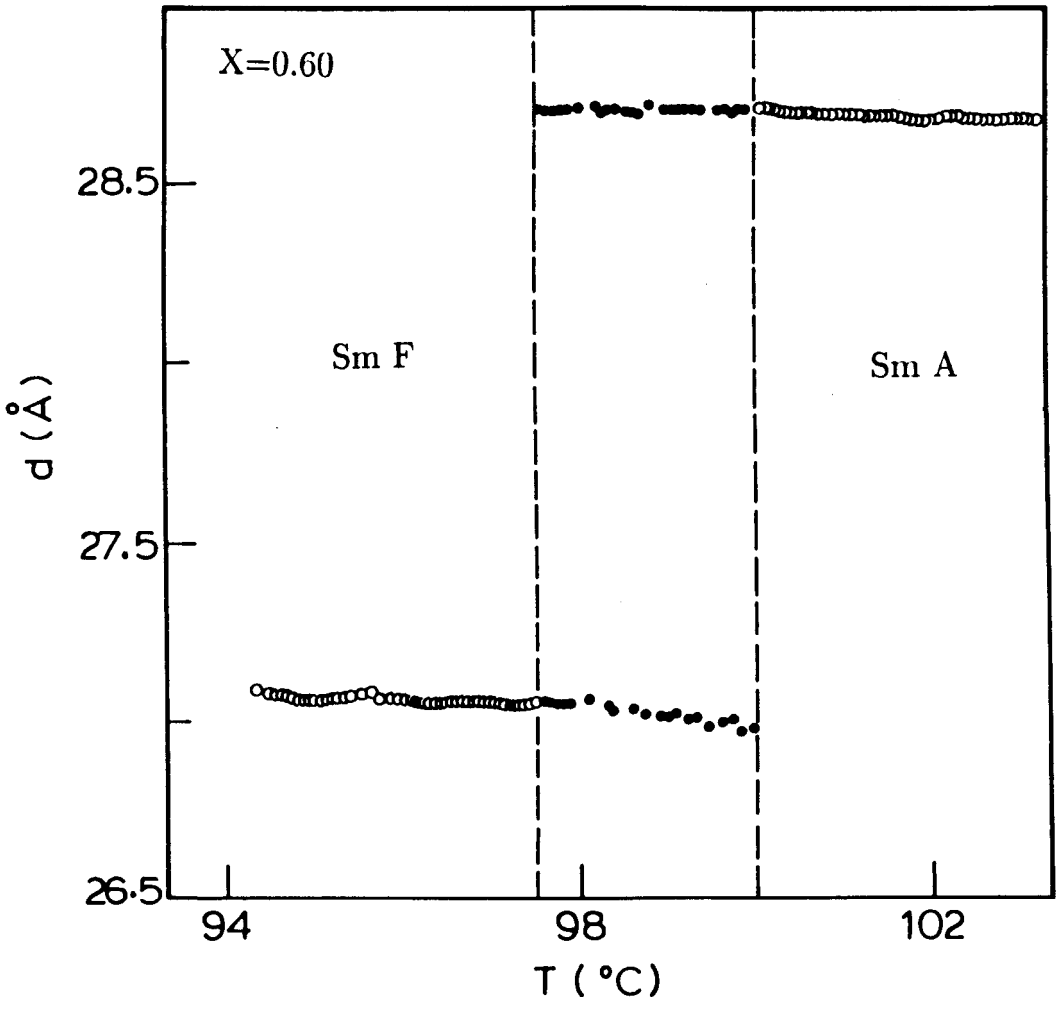

Figure 2.30: Thermal variation of d near Sm **A-Sm** F transition for X=0.60. The vertical clashed lines indicate the two-phase region.

to first order in tlie vicinity of the triple-point concentration. The Sm A phase temperature range for these mixtures was quite large($\simeq$ 18°C). This is somewhat puzzling in the light of known experimental results. The Sm A-Sm C transition is expected to become first order only when the temperature range of the Sm A phase is very small[18] and/or when the strength of the transverse dipole moment of the constituent molecule is very large.[17] In the present system neither of these two conditions are met and still the transition becomes first order. (Dielectric measurements[24] on TBBA has shown that the transverse dipole moment of the compound is extremely weak). One possible cause for this behaviour is the influence of tlie tilt field arising from the coupling between the BOO and the molecular tilt order parameter. Such a possibility still remains to be investigated theoretically.

References

[1] J.M.Kosterlitz and D.J.Thouless, *J.Phys.C:Solid State Phys.*, 6,1181 (1973); J.M.Kosterlitz, *J.Phys.C:Solid State Phys.*, 7, 1046 (1974).

[2] B.I.Halperin and D.R.Nelson, *Phys.Rev.Lett.*, 41, 121 (1978); D.R.Nelson and B.I.Halperin, *Phys.Rev.* B 19, 2457 (1979).

[3] A.P.Young, *Phys.Rev.***B 19**, 1855 (1979).

[4] R.J.Birgeneau and J.D.Litster, J.*Phys.Lett.(Paris)*, 39, L399 (1978).

[5] D.E.Moncton and R.Pindak, *Phys.Rev.Lett.*, 43, 701 (1979).

[6] R.Pindak, D.E.Moncton, S.C.Davey and J.W.Goodby, *Phys.Rev.Lett.*, 46, 1135 (1981).

[7] R.Bruinsma arid D.R.Nelson, *Phys.Rev.* B *23*, 402 (1981); D.R.Nelson and B.I.Halperin, *Phys.Rev.* B21, 5312 (1980).

[8] J.D.Brock, A.Aharony, R.J.Birgeneau, K.W.Evans-Lutterodt, J.D.Litster, P.M.Horn, G.B.Stephenson and A.R.Tajbakhsh, *Phys.Rev.Lett.*, 57, 98 (1986); J.D.Brock, D.Y.Noh, B.R.McClain, J.D.Litster, R.J.Birgeneau, A.Aharony, P.M.Horn and J.C.Liang, *Z.Phys.B Condensed matter*, 74, 197 (1989).

[9] A.Aharony, R.J.Birgeneau, J.D.Brock and J.D.Litster, *Phys.Rev.Lett.*, **57**, 1012 (1986).

[10] J.V.Selinger and D.R.Nelson, *Phys.Rev.Lett.*, 61, 416 (1988); J.V.Selinger and D.R.Nelson, *Phys.Rev.* A39, 3135 (1989).

[11] A.D.Defontaines and J.Prost, *Phys.Rev.* E 47, 1184 (1993).

[12] T. Pitchford, C. C. Huang, J. D. Budai, S. C. Davey, R. Pindak and J. W. Goodby, *Phys.Rev.* A34, 2422 (1986).

[13] G.Nounesis, R.Geer, H.Y.Liu, C.C.Huang and J.W.Goodby, *Phys.Rev.* **A 40**, 5468 (1989).

[14] Geetha G. Nair, V.N.Raja, S.Krishna Prasad, S.Chandrasekhar and B.K.Sadashiva, *Proceedings of the XIII AIRAPT International Conference on High Pressure Science and Technology,* Bangalore, Ed. A.K.Singh (Oxford & IBH) New delhi, 1992 p 523.

[15] P.G.de Gennes, *Mol. Cryst.* Liq. *Cryst.*, **21**, 49 (1973).

[16] S.C.Lien and C.C.Huang, *Phys.Rev.* A 30, 624 (1984).

[17] H.Y.Liu, C.C.Huang, T.Min, M.D.Wand, D.M. Walba, N.A.Clark, Ch.Bahr and G.Heppke, *Phys.Rev.* **A40**, 6759 (1989).

[18] S.Krishna Prasad, V.N.Raja, D.S Shankar Rao, Geetha G.Nair and M.E.Neubert, *Phys.Rev.* A42, 2479 (1990).

[19] The compounds TBBA and its higher homologues were kindly provided to us by Prof.M.E.Neubert.

[20] For a detailed discussion of the X-ray diffractometer setup with scintillation counter as the detector see Geetha G.Nair, Experimental studies on liquid crystalline phases and phase transitions Ph.D. Thesis, Bangalore University, 1992.

[21] C.Rosenblatt and J.T.Ho, *J.Physique*, 44, 383, 1983.

[22] Satyendra Kumar, *Phys.Rev.* **A23,** 3207 (1981).

[23] J.J.Benattar, F.Moussa and M.Lambert, *J.Chim.Phys.* 80, 99 (1983).

[24] L.Benguigi, Liquid crystals of one and two-dimensional Order, edited by W.Helfrich and G.Heppke(Springer-Verlag, Berlin, 1980) p 71.